iScience

CellPress
OPEN ACCESS

Article

Human iPSC modeling recapitulates *in vivo* sympathoadrenal development and reveals an aberrant developmental subpopulation in familial neuroblastoma

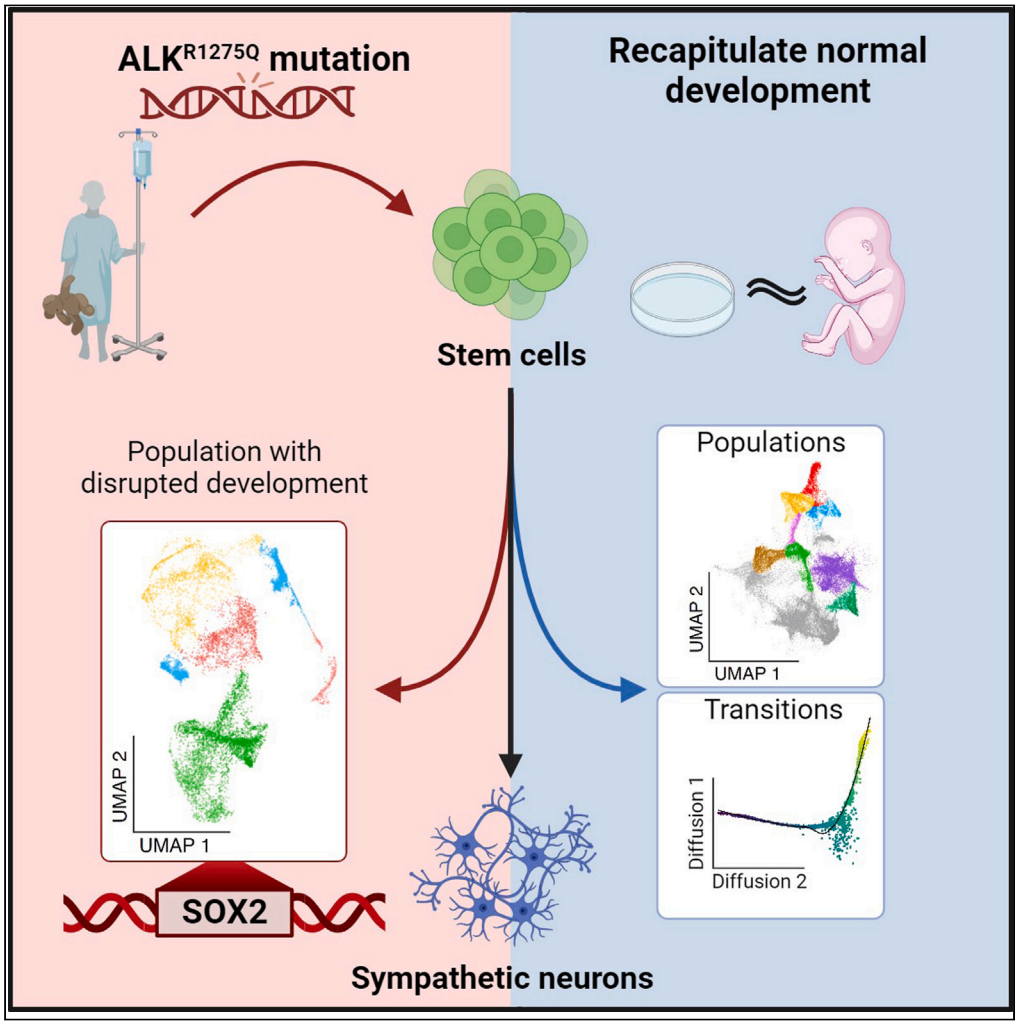

Stéphane Van Haver, Yujie Fan, Sarah-Lee Bekaert, ..., Lorenz Studer, Frank Speleman, Stephen S. Roberts

roberste@ohsu.edu

Highlights

An *in vitro* model to recapitulate the normal *in vivo* sympathoadrenal differentiation

Successfully capturing *in vivo* developmental complexity using *in vitro* modeling

A model for the study of early normal development and cancer pathogenesis

Analysis of patient-derived iPSCs identified an aberrant developmental subpopulation

Van Haver et al., iScience *27*, 108096
January 19, 2024
https://doi.org/10.1016/j.isci.2023.108096

iScience

CellPress
OPEN ACCESS

Article

Human iPSC modeling recapitulates *in vivo* sympathoadrenal development and reveals an aberrant developmental subpopulation in familial neuroblastoma

Stéphane Van Haver,[1,2] Yujie Fan,[3,4,9] Sarah-Lee Bekaert,[1,2] Celine Everaert,[1,2] Wouter Van Loocke,[1,2] Vittorio Zanzani,[1,11,12] Joke Deschildre,[1,11,12] Inés Fernandez Maestre,[13,14] Adrianna Amaro,[5] Vanessa Vermeirssen,[1,11,12] Katleen De Preter,[1,2] Ting Zhou,[10] Alex Kentsis,[5,6,7,8] Lorenz Studer,[3,4] Frank Speleman,[1,2,15] and Stephen S. Roberts[5,15,16,*]

SUMMARY

Studies defining normal and disrupted human neural crest cell development have been challenging given its early timing and intricacy of development. Consequently, insight into the early disruptive events causing a neural crest related disease such as pediatric cancer neuroblastoma is limited. To overcome this problem, we developed an *in vitro* differentiation model to recapitulate the normal *in vivo* developmental process of the sympathoadrenal lineage which gives rise to neuroblastoma. We used human *in vitro* pluripotent stem cells and single-cell RNA sequencing to recapitulate the molecular events during sympathoadrenal development. We provide a detailed map of dynamically regulated transcriptomes during sympathoblast formation and illustrate the power of this model to study early events of the development of human neuroblastoma, identifying a distinct subpopulation of cell marked by SOX2 expression in developing sympathoblast obtained from patient derived iPSC cells harboring a germline activating mutation in the anaplastic lymphoma kinase (ALK) gene.

INTRODUCTION

Neural crest cells (NCCs) are highly migratory transient progenitor cells, essential in early embryogenesis, that contribute to the development of numerous tissues including the peripheral nervous system. The ultimate developmental fate of these cells is largely determined by their migratory pathway and cranial-caudal anatomic location. One subset of NCCs migrates ventromedial to the dorsal aorta and are exposed to bone morphogenetic protein (BMP) signaling.[1–4] As a result, these multipotent truncal NCCs become lineage-restricted sympatho-adrenergic progenitors (SAPs) and ultimately give rise to the sympathetic ganglia and chromaffin cells of the adrenal medulla by approximately 16 weeks of gestation.[5–7] Given the early timing and intricacy of NCC development, studies defining normal human NCC development and its disruption have been challenging.[8–14] Given this difficulty, our understanding of human neural crest disorders remains limited. One of these disorders is the pediatric cancer neuroblastoma (NB), which is the most common extracranial solid tumor and the leading cause of cancer deaths in children under five years of age.[15–18] NB occurs anywhere along the developing sympathetic axis, but most frequently arise in the adrenal gland. Previous studies have shown that NB tumors express various markers of the sympathoadrenal lineage such as PHOX2B, HAND2, and GATA3. The expression of these markers in addition to the tumor's anatomical location, support the idea that disruption of normal sympathetic nervous development is likely to cause NB.[15,19]

[1]Department of Biomolecular Medicine, Ghent University, 9000 Ghent, Belgium
[2]Cancer Research Institute Ghent (CRIG), 9000 Ghent, Belgium
[3]The Center for Stem Cell Biology, Memorial Sloan Kettering Cancer Center (MSKCC), New York, NY, USA
[4]Developmental Biology Program, MSKCC, New York, NY 10065, USA
[5]Department of Pediatrics, MSKCC, New York, NY 10065, USA
[6]Molecular Pharmacology Program, MSKCC, New York, NY, USA
[7]Tow Center for Developmental Oncology, MSKCC, New York, NY 10065, USA
[8]Departments of Pediatrics, Pharmacology and Physiology & Biophysics, Weill Cornell Graduate School of Medical Sciences, Cornell University, New York, NY 10065, USA
[9]Weill Graduate School of Medical Sciences of Cornell University, New York, NY 10065, USA
[10]The SKI Stem Cell Research Facility, The Center for Stem Cell Biology and Developmental Biology Program, Sloan Kettering Institute, 1275 York Avenue, New York, NY 10065, USA
[11]Lab for Computational Biology, Integromics and Gene Regulation (CBIGR), Cancer Research Institute Ghent (CRIG), Ghent, Belgium
[12]Department of Biomedical Molecular Biology, Ghent University, 9000 Ghent, Belgium
[13]Human Oncology and Pathogenesis Program, Memorial Sloan Kettering Cancer Center, New York, NY, USA
[14]Louis V. Gerstner Jr Graduate School of Biomedical Sciences, Memorial Sloan Kettering Cancer Center, New York, NY, USA
[15]These authors contributed equally.
[16]Lead contact
*Correspondence: roberste@ohsu.edu
https://doi.org/10.1016/j.isci.2023.108096

Animal models such as the quail-chick embryo chimeras pioneered by Le Douarin et al. have been essential to our understanding of neural crest development.[20–23] Recently, several studies have utilized single-cell RNA sequencing (scRNA-seq) of human fetal tissue to further define the developmental landscape of the sympathoadrenal lineage.[24,25] These studies identified a series of intermediate cell types, which multipotent NCCs transition through until they terminally differentiate into mature adrenal chromaffin cells and sympathetic neurons. To enable better understanding of the dynamic interactions between these intermediate cell types and to study disordered sympatho-adrenergic development, we developed and characterized a human *in vitro* pluripotent stem cell-based model and characterized the sympathoadrenal development via sequential scRNA-seq. Further, we demonstrate the power of this novel model in studying early events in development of human NB by exploring the differences between normal cells and patient-specific induced pluripotent stem cells (iPSCs) derived from a child with familial NB harboring a germline mutation in the anaplastic lymphoma kinase (*ALK*) gene.[26–28]

RESULTS

An *in vitro* system to model sympatho-adrenergic development

While numerous protocols exist to generate NCCs *in vitro* from pluripotent stem cells,[29–32] the majority produce early migratory, multipotent NCCs. Additionally, most of these protocols produce cranial neural crest derivatives rather than caudal neural crest derivatives.[33] Few protocols have been developed to reliably generate lineage-restricted, non-cranial neural crest derivatives, such as sympathoblasts. Here we report an *in vitro* differentiation protocol to generate sympathoblasts from human iPSCs within 32 days (Figure 1A).

Using a modified dual SMAD inhibition approach,[34–36] we developed multipotent NCCs by day 16 of differentiation as evidenced by expression of SOX10 and FOXD3[30,37–39] (Figures 1B–1D). On day 16, we sorted by flow cytometry, CD49d^{+} cells to enrich for NCC. The expression of CD49d has been previously shown to specifically identify a SOX10^{+} multipotent NCC population.[40] To confirm the development of truncal NCCs, we determined HOX gene expression patterns within the first stage of the differentiation protocol and found the expected expression of truncal HOX genes, including *HOXB5/7/9*, with little to no expression of the more lumbar or caudal HOX genes (e.g., *HOXD9* and *HOXD11*) (Figure 1C). After enriching for NCCs, we then induced differentiation of the SAP lineage through BMP4/SMAD signaling on day 21. Activation of BMP4/SMAD signaling induced expression of the SAP core regulatory circuit (CRC), including rapid gene expression of the *ASCL1* pioneering transcription factor (TF), followed sequentially by the sympathetic lineage master regulator *PHOX2B*[41–43] along with that of other lineage-determining TFs, including *HAND2*, *GATA3*, *ISL1*, and *TBX2*, consistent with the expression patterns seen in previous studies of sympatho-adrenal development[44–47] (Figures 1D and S1). This induction of the CRC members is required for generating sympathoblasts during normal SAP differentiation.[48–52]

Later sympathoblast developmental markers, including *STMN2*, *ISL1* and *PRPH*,[25,47,53–56] widely expressed in the cell body and axons of neurons in the peripheral nervous system, steadily increased after induction of SAP development at day 21 (Figures 1D and S1). Since tyrosine hydroxylase (TH) is a marker of sympathoblast development,[57,58] we utilized a TH-tdTomato reporter line to validate the second part of the differentiation track (Figure 1A). TH positive cells were first detectable on day 28 and continued to increase as the differentiation progressed (Figure 1B). To further characterize this developmental progression, we performed gene set enrichment analysis (GSEA) for the differentially expressed genes across the differentiation track. In line with the above-described data, a comparison of day 35 (late SAP development) with day 16 (NCC stage) demonstrated enrichment of the chromaffin, SAP, and peripheral nervous system developmental datasets in day 35-cells (Figure S1). Notably, other NCC-derived signatures, such as those for melanocytes and osteoblasts, were not significantly enriched on day 35. Taken together, these transcription patterns substantiate the generation of SAPs from SOX10^{+} truncal NCCs that eventually differentiate into sympathetic neurons.

In vitro modeling recapitulates *in vivo* developmental complexity

Sympathoadrenal development is a complex process with cells progressing through numerous transitional states prior to reaching terminal differentiation.[24,25,59–62] Previous studies identify different developmental paths taken by extra-versus intra-adrenal sympathoblasts. Whilst the extra-adrenal sympathoblasts and sympathetic ganglia develop directly from NCCs, chromaffin cells and sympathoblasts in the adrenal gland arise from Schwann cell precursors (SCPs). Recent studies have described this intra-adrenal sympathoadrenal development process in further detail. We can infer that the developing cells will gradually transition from multipotent truncal NCCs to Schwann cell progenitors (SCPs),[63] which then further differentiate to either chromaffin cells or sympathoblasts.[24,25] Within the study of Jansky et al.[24] the transition from SCPs and bifurcation of the development into sympathoblasts and chromaffin cells was further divided into bridging cells and connecting progenitor cells (CPCs). The bridging cells consist of cells transitioning from the SCPs to chromaffin cells and sympathoblasts. These cells connect to a population named CPCs which spans the transcriptional space between bridge and chromaffin/neuroblast populations. During these transitions, external cues and dynamic regulatory networks guide the cells along the SAP developmental trajectory toward sympathoblasts. In addition to expression of the expected sympathoblast genes, the serial bulk RNA sequencing data also revealed gene expression signatures consistent with the other intermediate cell types previously identified in the *in vivo* SAP differentiation studies; for example, *PLP1*, a unique marker of the early developmental subpopulation of Schwann cell precursors (SCP), peaked on day 21.[24,25] The presence of these gene expression signatures suggested that our protocol may, in fact, be developing these intermediate cell types and not simply the expected "endpoint" sympathoblasts. Therefore, we next set out to determine whether our *in vitro* system replicated the *in vivo* dynamic complexity of SAP development. To accomplish this, we focused on defining the critical time frame for SAP development during the differentiation, as defined by expression changes of key genes including *ASCL1* and *PHOX2B*. This allowed us to identify a developmental window

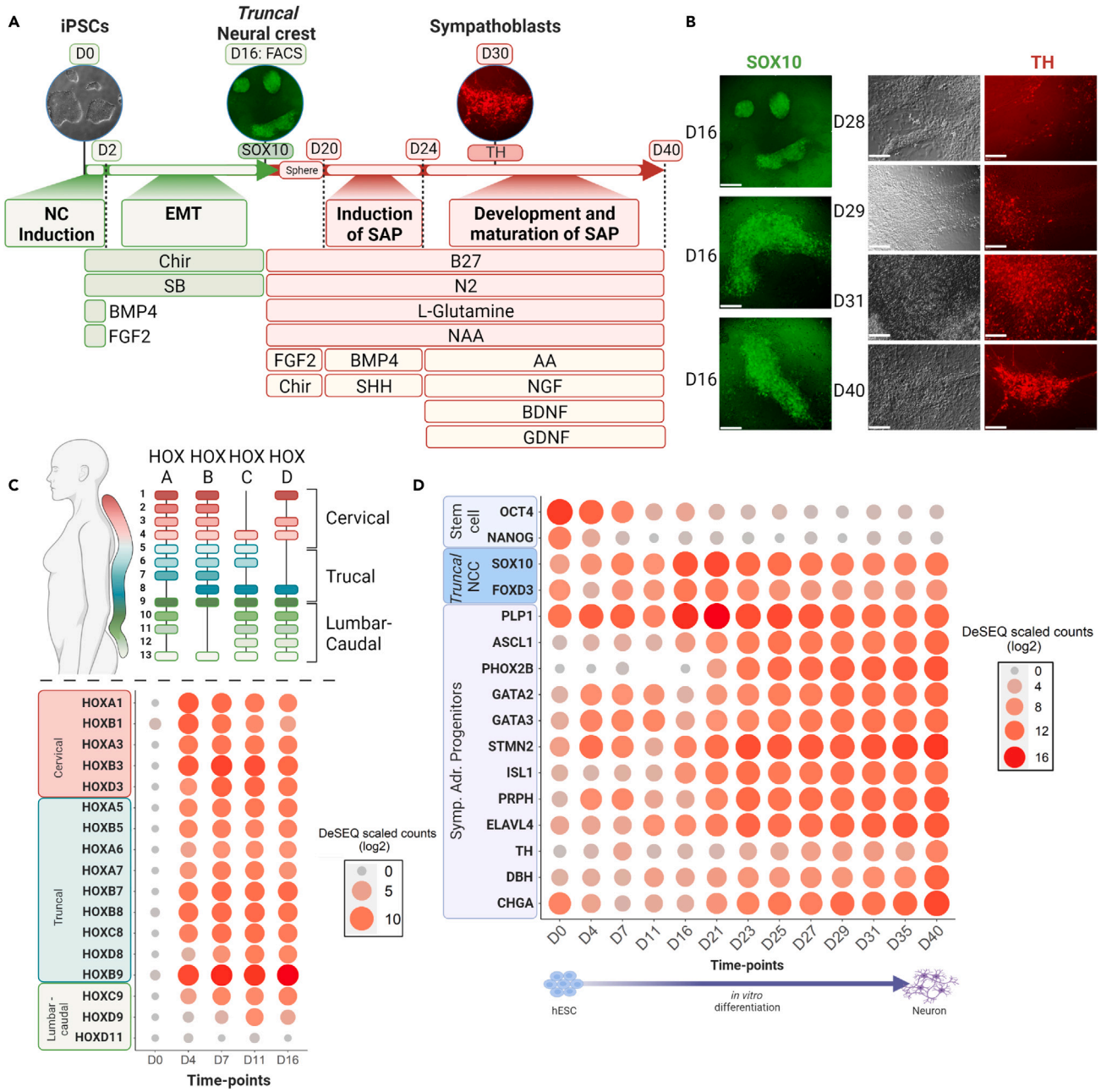

Figure 1. Analysis of key markers using a reporter cell line and bulk RNA sequencing confirms development of sympatho-adrenergic progenitors

(A) Schematic of the protocol used in the SAP differentiation model, the chemicals, and durations for each stage of the differentiation are indicated. D: day.

(B) Representative microscopic images of the SOX10-GFP (left) and TH-tdTomato (right) reporter cell lines. Scale bar: 250 μm; 4× magnification.

(C) Top: Overview figure indicating anterio-posterior localization associated with specific HOX gene expression; Bottom: Bubbleplot representing HOX gene expression based on sequential bulk RNA sequencing of samples, collected from J2 iPSCs and H9 hESC for a total of 4 biological replicates, at 13 time points representing the entirety of the differentiation process. The size and color of the spheres show the log2 scaled DeSEQ2 normalized counts. The x axis represents the time points of sample collection, with D0 being the stem cell stage, and D16 the day of FACS enrichment of NCC. The y axis shows the selected HOX genes associated with cervical, truncal and lumbar/caudal localization.

(D) Bubbleplot analogue to C, collected from J2 iPSCs and H9 hESC for a total of 4 biological replicates, showing on the y axis selected tissue specific markers indicative of developmental substage.

See also Figure S1.

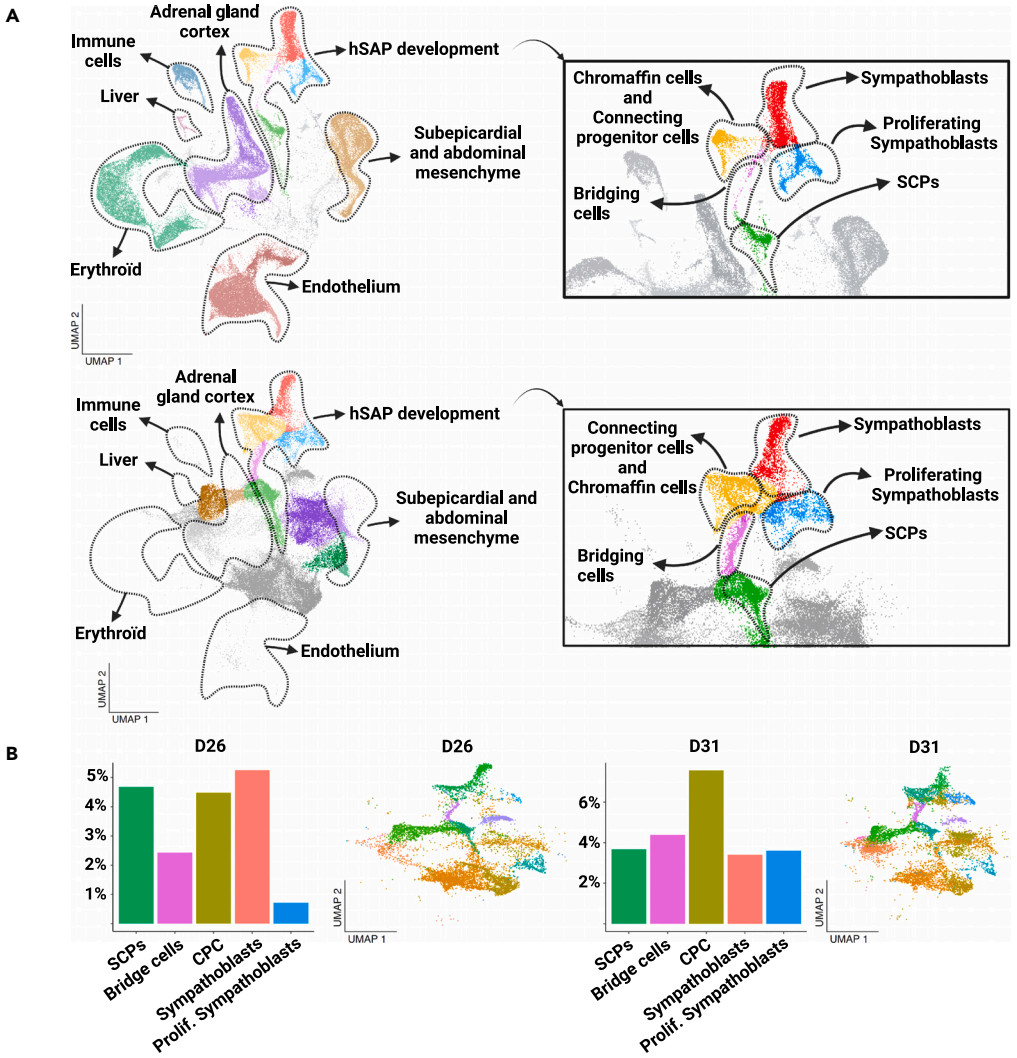

Figure 2. Comparison of human *in vitro* to human *in vivo* single cell data

(A) Top: UMAPs showing the *in vivo* samples from the Adameyko dataset after integration; Bottom: Mapping with the *in vitro* scRNA-seq data collected using the J2 iPSCs collected at 8 subsequent time-points (with for each time-point independent experiments). Both are color-coded by tissue type. The *in vivo* cells were visually separated from the *in vitro* cells. Top: *in vivo* data; the left panel annotated for the main tissue types and the right panel showing the SAP developmental subpopulations: Schwann cell precursors (SCP), bridging cells, chromaffin-like connecting progenitor cells (CPC) & chromaffin cells, and sympatho-adrenergic precursors (SAP). Bottom: *in vitro* data; part of the same analysis as A, now showing the separated *in vitro* cells. The left and right panels show the projection of the identified populations in *the in vivo* data.

(B) UMAPs for days 26 and 31 with therefrom calculated histograms showing the percentage of cells for the SAP developmental population.

See also Figure S2.

beginning on day 25 (after SAP induction) and ending on day 32 based on the increased expression of the later sympathoblasts developmental markers *PRPH*, *TH*, and *STMN2* (Figures 1D and S1).

To further explore the dynamic complexity suggested by the bulk RNA sequencing data, we performed serial scRNA-seq on our differentiating cells at eight successive time points throughout the developmental window indicated above. We then compared our scRNA-seq data to that obtained from *in vivo* samples by Kameneva et al.[25] using Uniform Manifold Approximation and Projection maps (UMAP) (Figure 2A). We observed that our *in vitro*-generated sympathoblasts, identified by the presence of developmental markers *STMN2*, *ISL1*, *PRPH*, *GAP43* and *ELAVL3/4*, mapped to the same population as their *in vivo* counterparts, signifying that their overall transcriptional profile closely resembles the *in vivo* population (Figures 2A and 3A). Strikingly, we could also clearly identify the SAP developmental subpopulations within the *in vitro*-derived cell populations. Specifically, we determined the developmental subpopulation of SCPs by the expression of the markers *SOX10*, *PLP1*, *ERBB3*, and *CDH19*, used in the study of Kameneva et al.[25] The first transition from SCP to sympathoblast/chromaffin cells, described in the study of Kameneva, was further explored in the study of Janksy et al.[24] In this transition they could further identify a bridging

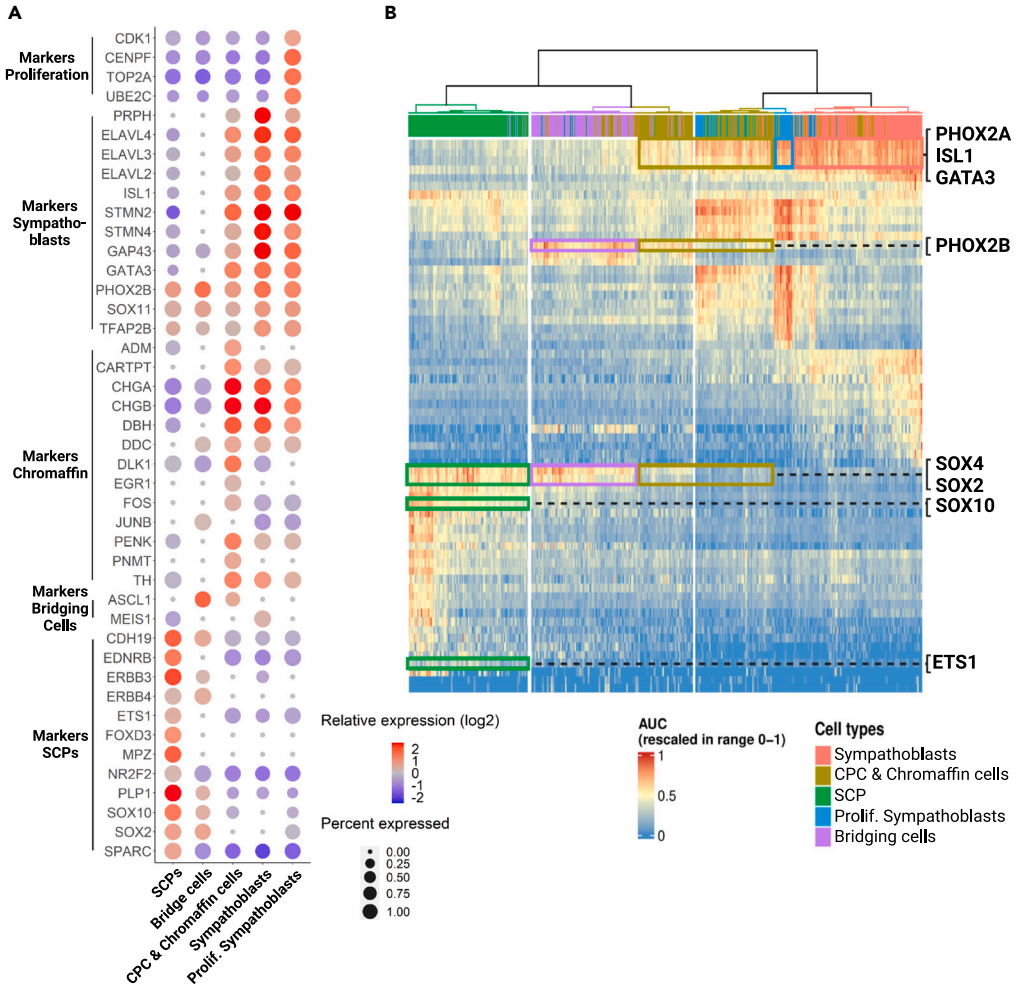

Figure 3. Validation of identified populations using key developmental markers

(A) Genes defining each tissue type. The color of the spheres indicating the log fold change, and their size, the percentage of the population expressing the gene.

(B) Heatmap of the gene regulatory network activity for the cells in the SAP developmental subpopulations, annotated by previously defined cell identities. AUC represents the activity scoring of the regulatory program associated with a specific TF.

See also Figures S3 and S4.

population connecting the SCPs with a population identified as CPCs. The CPCs were described by Jansky et al. to span the transcriptional space between bridge and chromaffin/neuroblast populations and reported to express markers of both, albeit on a lower level. When analyzing our *in vitro* data, using population markers identified in this study, we can identify the bridging cells, evident by the expression of *ASCL1*, specific to this population[24] (Figures 3A and S4). We could also identify the CPCs by the described expression of both chromaffin (*CHGA*+, *PENK*+) and sympathoblast (*ISL1*+, *STMN2*+) markers. However, the expression of established chromaffin cell markers such *CHGA* and *PNMT* indicates this population likely also includes early chromaffin cells (Figure 3A). Both *in vivo* and *in vitro*, there was a defined subpopulation of proliferating sympathoblast cells, identified by the expression of *TOP2A*, *UBE2C*, *CENPF*, and *CDK1*. We could not detect a separation between proliferating and non-proliferating cells within the other cell populations (Figure 3A). The total of the SAP developmental subpopulations represented 17.6% on day 26, and 22.7% on day 31 of all cells present in the differentiation. In general, the SAP developing cells were divided over the individual subpopulations ranging from 2.4 to 7.6% (Figures 2B and S2).

As expected, we also saw clear differences in the resulting populations between the *in vivo* and *in vitro* samples. The *in vivo* samples contained non-neuronal cell populations including immune cells, identified by *CD163* and *AIF1*; erythroid cells, marked by *HBB*, *ALAS2*, and *HBA2*; and endothelial cells expressing *KDR* and *PECAM1*. These non-neural crest derived cell types were not present in the *in vitro* derived samples. Conversely, we also identified cell populations within the *in vitro* derived samples that did not have a clear *in vivo* counterpart. This finding was not surprising, given the inherent limitations of a two-dimensional *in vitro* tissue culture system. In addition to the SAP developmental populations, we detected a distinct population of myofibroblast-like cells, identified by *TAGLN* and *ACTA2*; endoneurial fibroblasts, identified by *DCN* and *FBN1*; and melanocyte stem cells, identified by the expression of *DCT* and *PMEL*, representing 2.2%, 23.3% and 13.4%

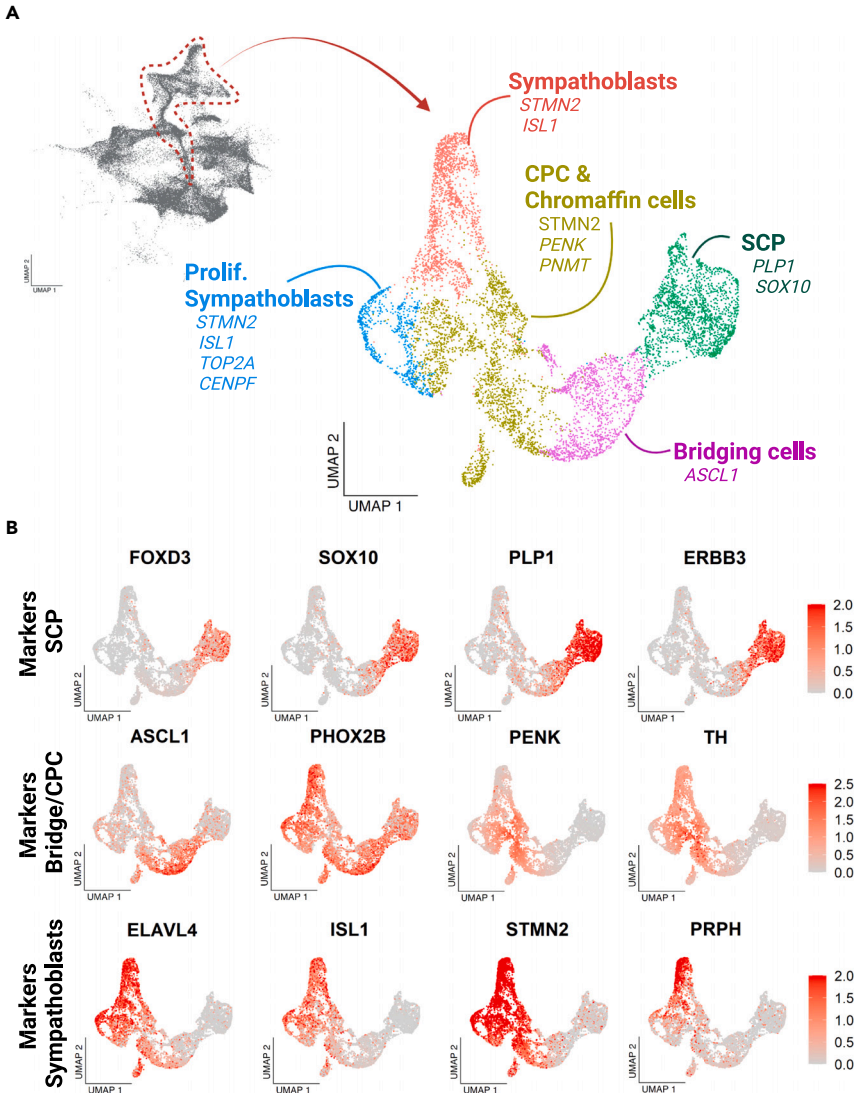

Figure 4. Reclustering of the cells of interest

(A) Left: UMAP indicating selection SAP developmental subpopulations for remapping and reclustering. Right: UMAP of reclustered SAP developmental subpopulations, color-coded by tissue type and annotated with key markers identifying the populations.

(B) UMAPs with developmental markers for the major SAP differentiating subpopulations. See also Figure S3 for additional marker analysis.

of the total cells, respectively. Additionally, we could not attribute known cell type-specific markers to 25.4% and 45% of the cells, on day 31 and 26, respectively. These unidentified cells may include *bona fide* transitioning cells, hitherto undetected subpopulations, as well as possible artifacts of the *in vitro* differentiation process (Figure S2).

The observation that the developmental sub-populations of interest resembled the *in vivo* cells led us to investigate whether there would also be similar dynamic changes and transitions between these populations. Analysis based on the activation of the gene regulatory network (GRN) showed cells of the same subpopulations grouping together, further confirming the cells identified in the SAP developmental subpopulations. The activity of the GRN also indicated overlap and transitions between the different subpopulations as described *in vivo* (Figure 3B). Next, to investigate the SAP cell fate transitions in more depth, we selected and re-clustered the transcriptomes of the identified SCP, bridging, CPC and sympathoblast cells in a similar fashion as the original dataset (Figure 4A). The resulting UMAP embedding showed that our SCPs (*PLP1*$^{+}$, *SOX10*$^{+}$, *SOX2*$^{+}$) were connected to CPCs (*PLP1*$^{-}$, *SOX10*$^{-}$, *ASCL1*$^{+}$, *HAND2*$^{+}$, *CHGA*$^{+}$, *PRPH*$^{-}$) through a bridging population (*PLP1*$^{+}$, *SOX10*$^{+}$, *ASCL1*$^{+}$, *HAND2*$^{+}$). CPCs then further connected to the sympathoblast cells (*PLP1*$^{-}$, *ASCL1*$^{-}$, *CHGA*$^{+}$, *STMN2*$^{+}$, *PRPH*$^{+}$), consistent with the previously described developmental progression (Figure 4B). To further analyze these developmental transitions, we also performed pseudotime analysis based on the diffusion distance of our identified cell populations (Figures 5A and 5B). As the starting point, we selected SCPs, as these represent the earliest developmental population of the SAP lineage. This targeted diffusion analysis

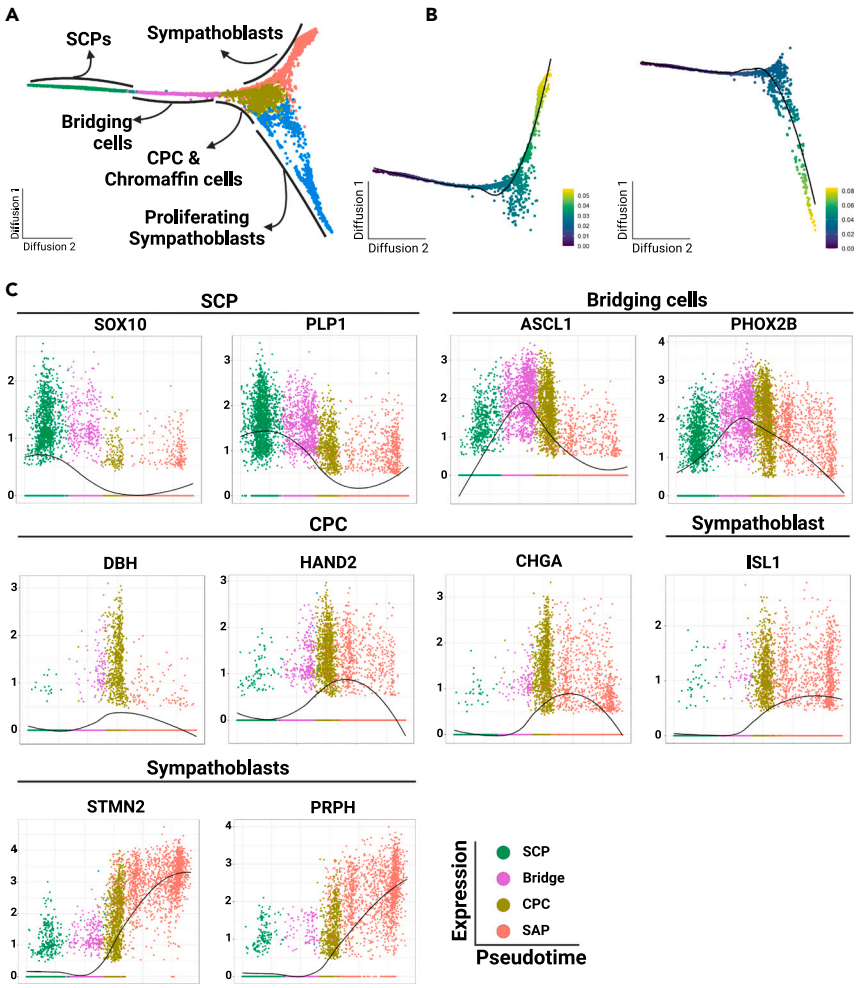

Figure 5. Developmental trajectories during *in vitro* differentiation

(A) Diffusion map of *in vitro* differentiating cells colored and annotated by cell population.

(B) Diffusion maps of *in vitro* differentiating cells colored by pseudotime trajectory as determined by slingshot. Top: showing SCP – sympathoblast pseudotime trajectory. Bottom: showing SCP – Proliferating sympathoblast pseudotime trajectory.

(C) Predicted expression in differentiating cells of developmental markers for SCP (*SOX10, PLP1*), Bridging cells (*ASCL1, PHOX2B*), CPC (*CHGA, DBH* and *HAND2*), sympathoblasts (*ISL1, STMN2* and *PRPH*) along the lineage trajectory shown in the diffusion plot, annotated for developmental subpopulation.

See also Figures S3 and S4.

confirmed the crosstalk between sympathoblast and SCPs via bridging cells and CPCs, at which point the trajectory bifurcated into non-proliferating and proliferating sympathoblast (Figures 5A and 5B). These transitions matched the *in vivo* results except for the expected absence of the chromaffin arm. The duration of BMP4 signaling in our differentiation protocol is optimized for the development of sympathoblasts, while generation of chromaffin cells would require longer exposure to BMP4.[64] Thus, generation of significant numbers of both endpoint populations at the same time in this *in vitro* protocol is not feasible. Developmental marker analysis indicates that a small number of chromaffin cells are likely grouped within the identified CPC population. Due to the lack of prolonged BMP4 signaling however, the protocol does not generate a clearly identifiable population of chromaffin cells. Analysis of developmental markers over pseudotime predicted the expected transitions of different markers within a developing cell along the signaling cascade. This cascade began with the downregulation of *PLP1*, *SOX10*, and *SOX2*, followed by upregulation of *ASCL1*, then immediately succeeded by upregulation of *PHOX2B*, which induces the further developmental signaling cascade and activation of later developmental markers, including *HAND2*, *CHGA*, *DBH*, *STMN2*, and *PRPH* (Figures 5C and S4). We also analyzed the regulatory programs of the GRN with high specificity scores defining the different SAP developmental populations (Figure S3). This analysis showed overlap between these specific regulatory programs only between the populations with predicted transitions, further confirming the dynamic changes we recapitulated *in vitro*. These analyses show that our model mirrors much of the complex and dynamic cellular heterogeneity seen *in vivo*, hence closely mimicking the normal developmental process.

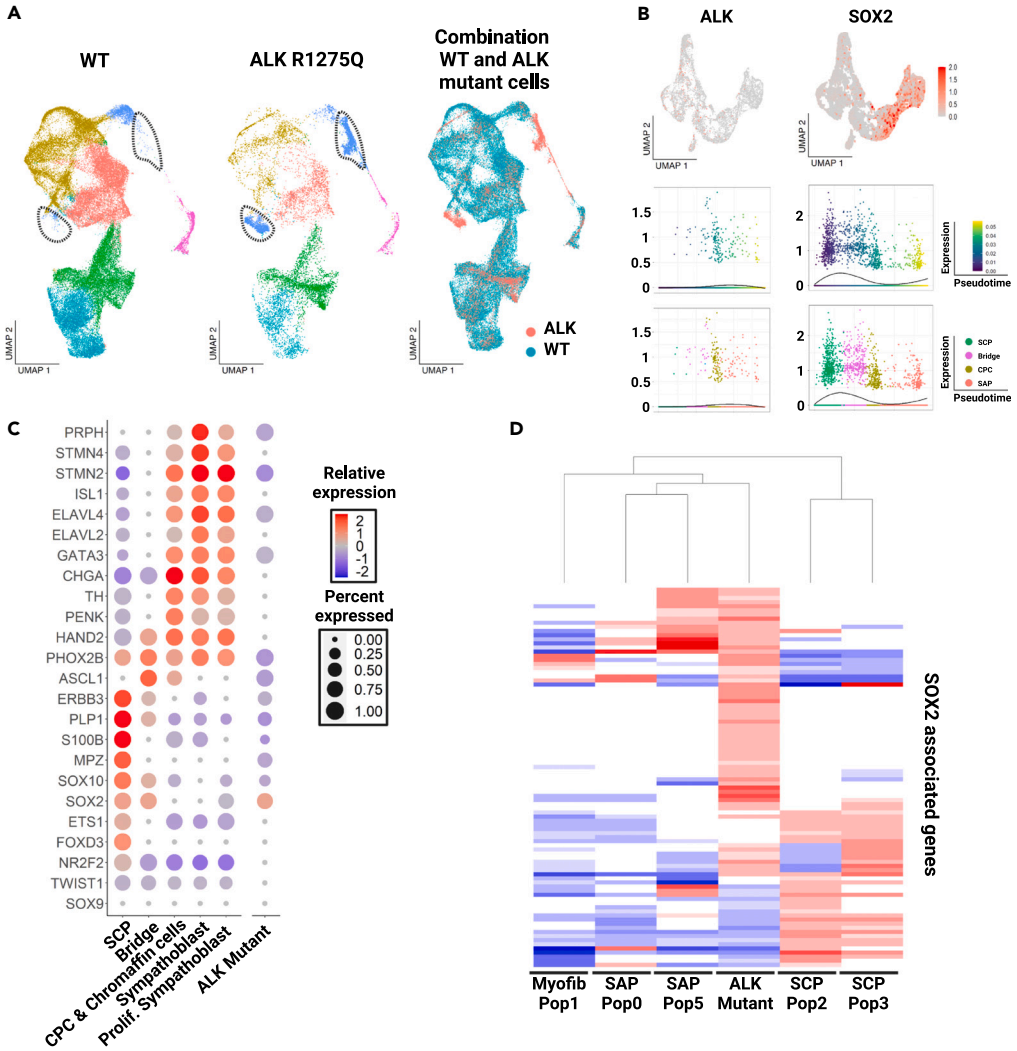

Figure 6. A unique SOX2^{+} ALK mutant population detected during development

(A) Left and Middle: UMAP indicating the distribution of WT cells (based on the scRNAseq of the J2 iPSCs for all 8 time-points) and ALK mutant cells (based on the scRNAseq of the NB05 iPSCs for all 4 time-points); Right: UMAP indicating the overlap between the sequenced time-points of both cell lines, annotated red for the ALK mutant cells and blue for WT cells (right). In the left and middle UMAPs, the population detected in ALK mutant cells only is highlighted with a dashed line.

(B) Top: UMAPS showing expression levels of *ALK* and *SOX2* as seen in the development of the WT cells; Bottom: Predicted expression along the lineage trajectory shown in the diffusion plot of Figure 5A and along the pseudotime shown in Figure 5B.

(C) Key developmental markers of NCC (*SOX9* and *TWIST1*), SCP (i.e., *SOX10, PLP1*), Bridging cells (*ASCL1*), CPC (i.e., *PENK, TH, CHGA*), SAP (i.e., *ISL1* and *STMN2*) for the different developmental populations, shared with between both cell lines, and the unique population detected only in the ALK mutant cell line.

(D) Heatmap showing the relative expression of known SOX2 target and associated genes for the populations identified in the UMAPS shown in Figures 5A and S7.

See also Figures S5 and S6.

Exploring the effect of ALK mutation on normal development using patient-specific iPS cells

Somatic mutations in the *ALK* gene are found in 8–10% of all human NB tumors. *ALK* germline mutations, although rare, were also shown to be responsible for most cases of familial NB.[26] However, how *ALK* specifically contributes to NB development remains unknown. To explore this question, we used our *in vitro* model to screen for differences in the SAP differentiation between wild-type (WT) iPSCs and a patient-specific iPSC line harboring an *ALK*^{R1275Q} mutation. We previously generated this iPSC line using peripheral blood mononuclear cells extracted from a child with familial NB (Figure S5).

Using the *ALK*^{R1275Q} mutant iPSCs, we performed serial scRNA-seq at four time points between days 25 and 32 following the same differentiation protocol. Next, we integrated the scRNA-seq data from these *ALK*^{R1275Q} mutant iPSCs with the previously generated WT iPSC-data for a comparative UMAP analysis. This revealed a large overlap between the *ALK*-mutant and WT populations, suggesting that the majority of *ALK*-mutant cells resemble their WT counterparts and undergo normal differentiation (Figures 6A and S7). This finding was not unexpected

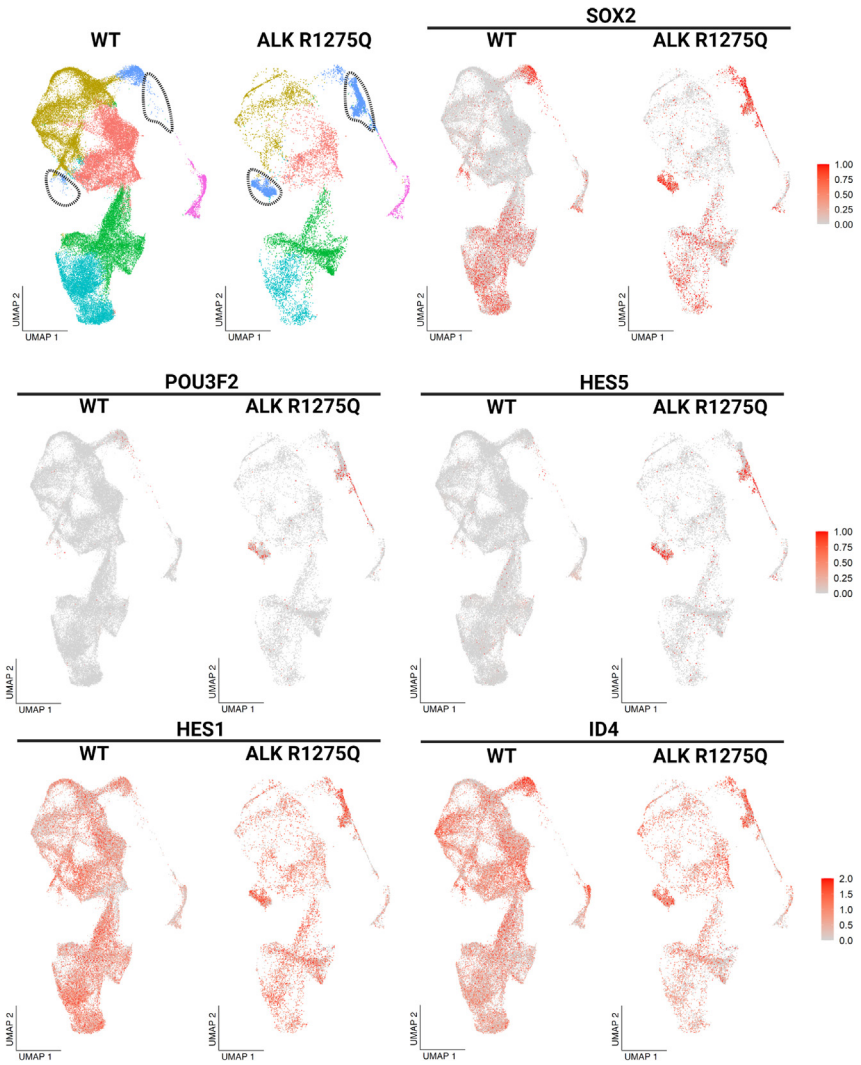

Figure 7. Expression of SOX2 target genes in the ALK mutant population

UMAP showing the expression of SOX2 target genes *POU3F2*, *HES1*, *HES5* and *ID4*. See also Figure S7 for additional marker analysis.

given that children with germline *ALK* mutations do not have a discernible abnormal developmental phenotype aside from an increased risk of developing NB.[26] However, despite these predominantly overlapping data, we did detect a distinct population of ALK^{R1275Q} mutant cells, representing 26.8% of total cells, that was absent in the WT population (Figure 6A). The ALK^{R1275Q} mutant cells had a normal morphology and appeared to differentiate normally through day 16, at which time point they appropriately expressed both *SOX2* and *SOX10* (Figure S6). However, upon further differentiation, the cells are expected to activate the pioneering TF gene *ASCL1* followed by *PHOX2B* and subsequently downregulate *SOX2* and *SOX10* as they further differentiate into the CPC stage. The developmental marker *SOX2* is critical during multipotent NCC development and is normally rapidly downregulated during further differentiation (Figure 6B). Indeed, *SOX10* was downregulated as expected, but there was persistence of SOX2 expression, along with a lack of upregulation of downstream differentiation markers (i.e., *ASCL1*, *PHOX2B* and *GATA3*) (Figure 6C). Further immunofluorescence staining at later stages in the differentiation (D35) showed an increased presence of *SOX2* positive cells in the ALK mutant differentiations compared to those in WT differentiations (Figure S6). Using a web-based TF enrichment analysis tool, ChEA3,[65] we identified *SOX2*, and its direct target gene *POU3F3*,[66] to be the most likely TFs responsible for the gene expression changes between the unique *ALK*-mutant population and the WT cells (Figure S6). We further investigated the genes enriched in the populations identified in the UMAP analysis (Figure 6A) by screening for known targets of *SOX2*, or genes positively correlated with *SOX2*. This analysis identified a set of *SOX2* target genes exclusively activated in the *ALK*-mutant population (Figure 6D). In addition to sustained expression of *SOX2*, we found upregulation of *POU3F2*, *POU3F3*, *HES1*, *HES5*, and *ID1* (Figures 6D and 7), all of which are characteristic of non-differentiating primitive neural progenitor cells, suggesting a disruption of differentiation and progenitor cell maintenance in this subpopulation.[67–71]

DISCUSSION

Embryonal malignancies of childhood, including NB, are best understood as disorders of abnormal development, with a failure of normal differentiation ultimately leading to oncogenic transformation. NB specifically represents a failure of sympathoadrenal development, but despite increasing insights into the underlying molecular pathogenesis, many questions remain unanswered. Human iPSC-based *in vitro* modeling represents a very versatile approach, with multiple applications being possible, including discovery of new disease mechanisms, as well as drug and toxicity screening.[72] In addition, for some tumors, including NB, the cell of origin may be difficult or impossible to isolate from human patients,[73] which hampers in depth analyses of critical genetic factors and perturbations driving or accompanying early tumor development. Since human iPSCs can generate unlimited numbers of patient-specific cells of any type, they can serve as an important source to overcome these challenges. Here we present a protocol for generating human sympathoblasts from human iPSCs, which have been proposed as progenitor cells for NB and give rise to adrenergic sympathetic neurons during normal development.

A major obstacle to the use of *in vitro* hPSC differentiation models to study differentiation mechanisms (as opposed to generation of "end-product" cell types) has been the inability to demonstrate how faithfully the *in vitro* differentiation actually mimics *in vivo* development. Our paper represents a first attempt to show that, in fact, it is possible to recapitulate a meaningful, if still incomplete, portion of the complexity of *in vivo* development using an *in vitro* hPSC based system. Within our differentiations, 17–22% of the cells present were part of the SAP developmental trajectory. This yield ranged from 2 to 7% for each of the developmental subpopulations of the *in vitro* generated cells (Figures 2B and S2). Of the remaining cells, 45% did not have an identifiable *in vivo* counterpart and lacked known cell type-specific markers on day 26, a percentage that reduced to 25.5% on day 31 (Figure S2). A subset of these cells expressed the NCC markers *TWIST1*, *ETS1*, *SOX10*, *FOXD3* and *LMO4*, indicating that a portion may be cells transitioning from the NCC to the SCP stage; these potential new subpopulations are only just beginning to be identified and characterized.[63]

Additionally, some cells present in the undefined population may represent an artifact of the differentiation process. This is not unexpected since *in vitro* differentiation is unlikely to exactly mimic the complexity of *in vivo* development. Another key feature of *in vivo* human developmental complexity is the dynamic interactions and transitions between developmental populations over time. Of note, we identified dynamic interactions similar to the *in vivo* context using diffusion mapping and pseudotime predictions. We also identified overlapping subgroups only between populations with predicted transitions, when analyzing regulatory programs of the GRN specific to the subpopulations. In particular, the SCPs and the bridging cells shared a set of regulatory programs, while bridging cells shared another group with the CPCs, and the CPCs shared two groups with both the non-proliferating and proliferating sympathoblasts (Figure S3). These overlapping regulatory programs validated the transitions predicted by the diffusion and pseudotime analyses, further confirming that our cells mimic the developmental dynamics observed during *in vivo* human development.

The fact that *in vivo* developmental complexity is largely recapitulated *in vitro* through our model underlines its potential to study human sympathetic nervous system development and related diseases. This model allows critical access to study the effect of early changes on normal development and NB pathogenesis. To highlight this, as "proof-of-principle", we used our model system to explore the impact of a germline ALK mutation on SAP development using a patient-specific iPSC line. Mutations in the *ALK* gene are responsible for most familial NB cases and somatic mutations in ALK are found in 8–10% of all NB tumors.[26–28,74] The *ALK* gene encodes a receptor tyrosine kinase that is normally expressed at high levels in the nervous system and was originally identified as a fusion protein with nucleophosmin in anaplastic large cell lymphoma (ALCL).[75] In NB, *ALK* point mutations within the tyrosine kinase domain, such as ALK^{R1275Q}, lead to constitutive receptor activation and persistent ALK signaling in the absence of ligand binding. Activation of ALK regulates cellular proliferation, differentiation, and apoptosis through different signaling pathways, including PI3K/AKT, RAS/MAPK and STAT3.[76–79] In NB, we and others have shown that signaling is predominantly governed through PI3K/AKT and RAS/MAPK and potentially important regulators (HBP1, ETV5, ERK5), thereby contributing to tumor formation.[80–82] Yet, deeper insights into the physiologic role and the mechanisms through which signaling by aberrantly activated ALK can promote NB development require further studies and appropriate models.[83–86] Using scRNA-seq analysis of the iPSC-derived ALKR1275Q-mutant cells uncovered an abnormal subpopulation consisting of cells that lacked critical differentiation markers, including SOX10, PLP1, ASCL1, STMN2, and ISL1, but maintained the expression of one developmental marker, SOX2 (Figure 6C). Additional immunofluorescence staining at late stage differentiation showed the increased presence of SOX2 positive cells in the ALK mutant differentiations (Figure S6). Of further importance, a substantial proportion of differentiated ALK-mutant iPSCs (~25%) exhibit this abnormal development (Figure S7). Why the remaining *ALK*-mutant cells appeared to differentiate completely normally needs to be studied in further detail but correlates with the normal sympathetic neuronal developmental phenotype in patients with germline *ALK* mutations.

SOX2 has crucial roles in embryogenesis and development,[87–89] making its increased expression in the mutant population of particular interest. SOX2 expression, present during early development of the NCCs and SCPs, is downregulated upon further maturation and development (Figure 6B). Misexpression of SOX2 during this developmental process can block neuronal differentiation and maintain the progenitor population.[90–93] More specifically, SOX2 antagonizes the neuronal differentiation induced by ASCL1,[90,94] which is a critical pioneering TF inducing the signaling cascade to allow the cells to transition further along the SAP developmental pathway. The SOX2 downstream targets identified in the subpopulation, such as HES1 and HES5, play essential roles during early neural development, with their expression decreasing during further differentiation.[70,71] Specifically, they maintain the number and status of undifferentiated neural stem cells and neural progenitors.[67–69] Additionally, they can repress the expression and activity of ASCL1, thereby inhibiting neuronal differentiation.[95] We also noticed induction of the gene *ID4*, whose protein product is known to drive the proliferation of neural stem cells.[96] The genes coding for the POU proteins POU3F2 (*BRN2*) and POU3F3 (*BRN1*), reported to co-localize with SOX2 expression in neural progenitor cells,[66] were also

upregulated. Their expression is mainly restricted to early neural development[97–99] and they are thought to repress BMP signaling.[100] Importantly, SOX2 expression has been linked to a primitive, aggressive phenotype and worse prognosis in several human cancers, including lung cancer, glioblastoma, and NB.[101–103] In NB, expression of SOX2 is associated with a stem cell-like phenotype, aggressive clinical behavior, and poor prognosis. Further, expression of the ALK fusion oncoprotein in ALK-positive ALCL induces expression of SOX2, leading to an immature phenotype and aggressive cancer cell behavior.[104,105] Using single cell transcriptome analysis we were able to trace where and how *ALK*-mutant cells diverge from their normal trajectory, which had up to now been unfeasible. Based on our analysis, we hypothesize that constitutive ALK signaling may cause aberrant expression of *SOX2* and its target genes in a subset of NCCs. This alteration may, in turn, lead to repression of critical BMP signaling and subsequent failure of activation of ASCL1. As a result of this failure, there is blockage in NCC differentiation. NCCs are thus maintained as an abnormal early progenitor population that may be more susceptible to acquisition of further mutations and ultimately oncogenic transformation to NB.

An alternative explanation, in light of previous studies showing inhibition of neural crest induction upon sustained expression of SOX2, is that the unique population of cells found in the ALK^{R1275Q} mutant cell line represent aberrant central nervous system neuroepithelial cells.[106,107] Gene expression analysis did identify central nervous system genes (*FOXG1*, *NR2E1*, *SALL3)* in the specific ALK mutant population. However, the fact that these cells were derived from an FACS-sorted population of SOX10+ NCCs suggests that they more likely represent aberrant neural crest derivatives than abnormal CNS progenitor cells. Importantly, these experiments highlight the ability of this model to generate and explore new biological insights that current animal models cannot. To confirm the origin of these cells and their role in NB development will require further in-depth mechanistic studies.

In summary, our work here demonstrates the power of combining patient-specific iPSCs, dynamic *in vitro* developmental modeling, and analysis at single cell resolution to explore both normal and abnormal SAP development.

Limitations of the study

While our *in vitro* model allowed us to work with human iPSCs to model sympathetic nervous development, the two-dimensional tissue culture system remains an artificial environment that cannot fully capture the complex environment of a developing organism. To ameliorate this limitation, our model can be used in conjunction with *in vivo* systems where cells generated by our model can be applied to *in vivo* experiments using transplantation based methods. Despite this disadvantage, our model does generate the different SAP developmental subpopulations with a current efficiency of 17–22% and mimic the *in vivo* dynamic complexity. Efforts to improve the yield of the differentiation and to purify and characterize the subpopulations of interest are on-going. The use of the patient specific ALK^{R1275Q}-mutant cell line shows the potential of our model to study human sympatho-adrenergic development. However, further in-depth mechanistic studies will be required to confirm the hypothesis we formulated here.

STAR★METHODS

Detailed methods are provided in the online version of this paper and include the following:

- KEY RESOURCES TABLE
- RESOURCE AVAILABILITY
  - Lead contact
  - Materials availability
  - Data and code availability
- EXPERIMENTAL MODEL AND STUDY PARTICIPANT DETAILS
  - Human subjects
  - Cell lines
  - Coating of culture plates
  - Culturing of PSCs
- METHOD DETAILS
  - Generating patient-specific iPSCs
  - Validation of pluripotency of generated patient-specific iPSC
  - Differentiation of PSC to hSAPs
  - Immunofluorescence (IF) imaging
  - Bulk RNAseq
  - Cell hashing
  - 10X genomics data generation and sequencing
  - Biological replicates in experimental design
- QUANTIFICATION AND STATISTICAL ANALYSIS
  - Gene and HTO quantification
  - Quality control, normalization and integration
  - Cell type annotation
  - Pseudotime analysis

- Regulatory program activity in single cells
- Gene set enrichment analysis

SUPPLEMENTAL INFORMATION

Supplemental information can be found online at https://doi.org/10.1016/j.isci.2023.108096.

ACKNOWLEDGMENTS

- The first author is supported by a grant for fundamental research of the Research Foundation – Flanders no 11D8120N.
- This research was funded in part through the NIH/NCI Cancer Center Support Grant P30 CA008748.
- We acknowledge the use of the Integrated Genomics Operation Core at MSKCC, funded by the NCI Cancer Centre Support Grant (CCSG, P30 CA08748), Cycle for Survival, and the Marie-Josée and Henry R. Kravis Centre for Molecular Oncology.
- We acknowledge the use of the Single-cell Analysis Innovation Lab (SAIL) at MSKCC.
- We acknowledge the use of the Flow Cytometry Core Facility at MSKCC, funded by the NCI Cancer Center Support Grant (CCSG, P30 CA08748).
- Figures were created with Biorender.com.
- A.K. acknowledges support of NIH R01 CA214812; he is a Scholar of the Leukemia & Lymphoma Society.
- We acknowledge Inés Fernandez Maestre for reviewing and editing the manuscript.

AUTHOR CONTRIBUTIONS

Conceptualization, S.S.R., F.S., and S.V.H.; Methodology, Y.F. and L.S.; Investigation, S.V.H.; Formal analysis S.V.H., W.V.L., S.B., C.E., V.Z., J.D., and V.V.; Data Curation, S.B; Resources, T.Z., A.K., L.S., S.S.R., and F.S.; Writing – Original Draft, S.V.H.; Writing – Review and Editing, I.F.M., A.A., S.S.R., F.S., L.S., A.K., T.Z., K.D.P., V.V., J.D., V.Z., W.V.L., C.E., S.B., and Y.F.; Visualization, S.V.H.; Supervision, S.S.R. and F.S.; Project Administration, S.S.R., F.S., and S.V.H.; Funding Acquisition, S.S.R. and F.S.

DECLARATION OF INTERESTS

A.K. is a consultant to Novartis, Rgenta, and Blueprint Medicines. L.S. is a scientific co-founder and consultant of Bluerock Therapeutics Inc. All other authors declare no conflict of interest.

Received: December 20, 2022
Revised: June 12, 2023
Accepted: September 26, 2023
Published: September 30, 2023

REFERENCES

1. Britsch, S., Li, L., Kirchhoff, S., Theuring, F., Brinkmann, V., Birchmeier, C., and Riethmacher, D. (1998). The ErbB2 and ErbB3 receptors and their ligand, neuregulin-1, are essential for development of the sympathetic nervous system. Gene Dev. *12*, 1825–1836. https://doi.org/10.1101/gad.12.12.1825.
2. Huber, K. (2006). The sympathoadrenal cell lineage: specification, diversification, and new perspectives. Dev. Biol. *298*, 335–343. https://doi.org/10.1016/j.ydbio.2006.07.010.
3. Kasemeier-Kulesa, J.C., McLennan, R., Romine, M.H., Kulesa, P.M., and Lefcort, F. (2010). CXCR4 controls ventral migration of sympathetic precursor cells. J. Neurosci. *30*, 13078–13088. https://doi.org/10.1523/JNEUROSCI.0892-10.2010.
4. Saito, D., Takase, Y., Murai, H., and Takahashi, Y. (2012). The Dorsal Aorta Initiates a Molecular Cascade That Instructs Sympatho-Adrenal Specification. Science *336*, 1578–1581. https://doi.org/10.1126/science.1222369.
5. Huber, K., Kalcheim, C., and Unsicker, K. (2009). The development of the chromaffin cell lineage from the neural crest. Auton. Neurosci. *151*, 10–16. https://doi.org/10.1016/j.autneu.2009.07.020.
6. Marshall, G.M., Carter, D.R., Cheung, B.B., Liu, T., Mateos, M.K., Meyerowitz, J.G., and Weiss, W.A. (2014). The prenatal origins of cancer. Nat. Rev. Cancer *14*, 277–289. https://doi.org/10.1038/nrc3679.
7. Unsicker, K., Huber, K., Schober, A., and Kalcheim, C. (2013). Resolved and open issues in chromaffin cell development. Mech. Dev. *130*, 324–329. https://doi.org/10.1016/j.mod.2012.11.004.
8. Bhatt, S., Diaz, R., and Trainor, P.A. (2013). Signals and switches in Mammalian neural crest cell differentiation. Cold Spring Harb. Perspect. Biol. *5*, a008326. https://doi.org/10.1101/cshperspect.a008326.
9. Carmona-Fontaine, C., Matthews, H., and Mayor, R. (2008). Directional cell migration *in vivo* Wnt at the crest. Cell Adh. Migr. *2*, 240–242. https://doi.org/10.4161/cam.2.4.6747.
10. Carmona-Fontaine, C., Matthews, H.K., Kuriyama, S., Moreno, M., Dunn, G.A., Parsons, M., Stern, C.D., and Mayor, R. (2008). Contact inhibition of locomotion *in vivo* controls neural crest directional migration. Nature *456*, 957–961. https://doi.org/10.1038/nature07441.
11. Green, S.A., Simoes-Costa, M., and Bronner, M.E. (2015). Evolution of vertebrates as viewed from the crest. Nature *520*, 474–482. https://doi.org/10.1038/nature14436.
12. Kasemeier-Kulesa, J.C., Kulesa, P.M., and Lefcort, F. (2005). Imaging neural crest cell dynamics during formation of dorsal root ganglia and sympathetic ganglia. Development *132*, 235–245. https://doi.org/10.1242/dev.01553.
13. Krull, C.E., Lansford, R., Gale, N.W., Collazo, A., Marcelle, C., Yancopoulos, G.D., Fraser, S.E., and BronnerFraser, M. (1997). Interactions of Eph-related receptors and ligands confer rostrocaudal pattern to trunk neural crest migration. Curr. Biol. *7*, 571–580. https://doi.org/10.1016/S0960-9822(06)00256-9.
14. Perris, R. (1997). The extracellular matrix in neural crest-cell migration. Trends Neurosci. *20*, 23–31. https://doi.org/10.1016/S0166-2236(96)10063-1.
15. Maris, J.M. (2010). Medical Progress: Recent Advances in Neuroblastoma. N. Engl. J. Med. *362*, 2202–2211. https://doi.org/10.1056/NEJMra0804577.
16. Maris, J.M., Hogarty, M.D., Bagatell, R., and Cohn, S.L. (2007). Neuroblastoma. Lancet

369, 2106–2120. https://doi.org/10.1016/S0140-6736(07)60983-0.
17. Matthay, K.K., Maris, J.M., Schleiermacher, G., Nakagawara, A., Mackall, C.L., Diller, L., and Weiss, W.A. (2016). Neuroblastoma. Nat. Rev. Dis. Primers *2*, 16078. https://doi.org/10.1038/nrdp.2016.78.
18. Padovan-Merhar, O.M., Raman, P., Rubnitz, K.R., Ali, S.M., Miller, V.A., Mosse, Y.P., Granger, M.P., Weiss, B.D., Maris, J.M., and Modak, S. (2016). Enrichment of targetable mutations in the relapsed neuroblastoma genome. Cancer Res. *76*, 2431. https://doi.org/10.1158/1538-7445.Am2016-2431.
19. Boeva, V., Louis-Brennetot, C., Peltier, A., Durand, S., Pierre-Eugène, C., Raynal, V., Etchevers, H.C., Thomas, S., Lermine, A., Daudigeos-Dubus, E., et al. (2017). Heterogeneity of neuroblastoma cell identity defined by transcriptional circuitries. Nat. Genet. *49*, 1408–1413. https://doi.org/10.1038/ng.3921.
20. Le Douarin, N.M., and Teillet, M.A. (1974). Experimental analysis of the migration and differentiation of neuroblasts of the autonomic nervous system and of neurectodermal mesenchymal derivatives, using a biological cell marking technique. Dev. Biol. *41*, 162–184. https://doi.org/10.1016/0012-1606(74)90291-7.
21. Bronnerfraser, M., and Fraser, S.E. (1988). Cell Lineage Analysis Reveals Multipotency of Some Avian Neural Crest Cells. Nature *335*, 161–164. https://doi.org/10.1038/335161a0.
22. Le Douarin, N.M., and Dupin, E. (2018). The "beginnings" of the neural crest. Dev. Biol. *444* (*Suppl 1*), S3–S13. https://doi.org/10.1016/j.ydbio.2018.07.019.
23. Noden, D.M. (1975). An analysis of migratory behavior of avian cephalic neural crest cells. Dev. Biol. *42*, 106–130. https://doi.org/10.1016/0012-1606(75)90318-8.
24. Jansky, S., Sharma, A.K., Körber, V., Quintero, A., Toprak, U.H., Wecht, E.M., Gartlgruber, M., Greco, A., Chomsky, E., Grünewald, T.G.P., et al. (2021). Single-cell transcriptomic analyses provide insights into the developmental origins of neuroblastoma. Nat. Genet. *53*, 683–693. https://doi.org/10.1038/s41588-021-00806-1.
25. Kameneva, P., Artemov, A.V., Kastriti, M.E., Faure, L., Olsen, T.K., Otte, J., Erickson, A., Semsch, B., Andersson, E.R., Ratz, M., et al. (2021). Single-cell transcriptomics of human embryos identifies multiple sympathoblast lineages with potential implications for neuroblastoma origin. Nat. Genet. *53*, 694–706. https://doi.org/10.1038/s41588-021-00818-x.
26. Mosse, Y.P., Laudenslager, M., Longo, L., Cole, K.A., Wood, A., Attiyeh, E.F., Laquaglia, M.J., Sennett, R., Lynch, J.E., Perri, P., et al. (2008). Identification of ALK as a major familial neuroblastoma predisposition gene. Nature *455*, 930–935. https://doi.org/10.1038/nature07261.
27. Janoueix-Lerosey, I., Lequin, D., Brugières, L., Ribeiro, A., de Pontual, L., Combaret, V., Raynal, V., Puisieux, A., Schleiermacher, G., Pierron, G., et al. (2008). Somatic and germline activating mutations of the ALK kinase receptor in neuroblastoma. Nature *455*, 967–970. https://doi.org/10.1038/nature07398.
28. George, R.E., Sanda, T., Hanna, M., Fröhling, S., Luther, W., 2nd, Zhang, J., Ahn, Y., Zhou, W., London, W.B., McGrady, P., et al. (2008). Activating mutations in ALK provide a therapeutic target in neuroblastoma. Nature *455*, 975–978. https://doi.org/10.1038/nature07397.
29. Kreitzer, F.R., Salomonis, N., Sheehan, A., Huang, M., Park, J.S., Spindler, M.J., Lizarraga, P., Weiss, W.A., So, P.L., and Conklin, B.R. (2013). A robust method to derive functional neural crest cells from human pluripotent stem cells. Am. J. Stem Cells *2*, 119–131.
30. Lee, G., Chambers, S.M., Tomishima, M.J., and Studer, L. (2010). Derivation of neural crest cells from human pluripotent stem cells. Nat. Protoc. *5*, 688–701. https://doi.org/10.1038/nprot.2010.35.
31. Menendez, L., Kulik, M.J., Page, A.T., Park, S.S., Lauderdale, J.D., Cunningham, M.L., and Dalton, S. (2013). Directed differentiation of human pluripotent cells to neural crest stem cells. Nat. Protoc. *8*, 203–212. https://doi.org/10.1038/nprot.2012.156.
32. Mica, Y., Lee, G., Chambers, S.M., Tomishima, M.J., and Studer, L. (2013). Modeling neural crest induction, melanocyte specification, and disease-related pigmentation defects in hESCs and patient-specific iPSCs. Cell Rep. *3*, 1140–1152. https://doi.org/10.1016/j.celrep.2013.03.025.
33. Huang, M., Miller, M.L., McHenry, L.K., Zheng, T., Zhen, Q., Ilkhanizadeh, S., Conklin, B.R., Bronner, M.E., and Weiss, W.A. (2016). Generating trunk neural crest from human pluripotent stem cells. Sci. Rep. *6*, 19727. https://doi.org/10.1038/srep19727.
34. Chambers, S.M., Mica, Y., Lee, G., Studer, L., and Tomishima, M.J. (2016). Dual-SMAD Inhibition/WNT Activation-Based Methods to Induce Neural Crest and Derivatives from Human Pluripotent Stem Cells. Methods Mol. Biol. *1307*, 329–343. https://doi.org/10.1007/7651_2013_59.
35. Menendez, L., Yatskievych, T.A., Antin, P.B., and Dalton, S. (2011). Wnt signaling and a Smad pathway blockade direct the differentiation of human pluripotent stem cells to multipotent neural crest cells. Proc. Natl. Acad. Sci. USA *108*, 19240–19245. https://doi.org/10.1073/pnas.1113746108.
36. Chambers, S.M., Fasano, C.A., Papapetrou, E.P., Tomishima, M., Sadelain, M., and Studer, L. (2009). Highly efficient neural conversion of human ES and iPS cells by dual inhibition of SMAD signaling. Nat. Biotechnol. *27*, 275–280. https://doi.org/10.1038/nbt.1529.
37. Reiprich, S., Stolt, C.C., Schreiner, S., Parlato, R., and Wegner, M. (2008). SoxE proteins are differentially required in mouse adrenal gland development. Mol. Biol. Cell *19*, 1575–1586. https://doi.org/10.1091/mbc.E07-08-0782.
38. Southard-Smith, E.M., Kos, L., and Pavan, W.J. (1998). Sox10 mutation disrupts neural crest development in Dom Hirschsprung mouse model. Nat. Genet. *18*, 60–64. https://doi.org/10.1038/ng0198-60.
39. Britsch, S., Goerich, D.E., Riethmacher, D., Peirano, R.I., Rossner, M., Nave, K.A., Birchmeier, C., and Wegner, M. (2001). The transcription factor Sox10 is a key regulator of peripheral glial development. Gene Dev. *15*, 66–78. https://doi.org/10.1101/gad.186601.
40. Fattahi, F., Steinbeck, J.A., Kriks, S., Tchieu, J., Zimmer, B., Kishinevsky, S., Zeltner, N., Mica, Y., El-Nachef, W., Zhao, H., et al. (2016). Deriving human ENS lineages for cell therapy and drug discovery in Hirschsprung disease. Nature *531*, 105–109. https://doi.org/10.1038/nature16951.
41. Anderson, D.J. (1993). Molecular control of cell fate in the neural crest: the sympathoadrenal lineage. Annu. Rev. Neurosci. *16*, 129–158. https://doi.org/10.1146/annurev.ne.16.030193.001021.
42. Schneider, C., Wicht, H., Enderich, J., Wegner, M., and Rohrer, H. (1999). Bone morphogenetic proteins are required *in vivo* for the generation of sympathetic neurons. Neuron *24*, 861–870. https://doi.org/10.1016/s0896-6273(00)81033-8.
43. Takahashi, Y., Sipp, D., and Enomoto, H. (2013). Tissue interactions in neural crest cell development and disease. Science *341*, 860–863. https://doi.org/10.1126/science.1230717.
44. Coppola, E., d'Autréaux, F., Rijli, F.M., and Brunet, J.F. (2010). Ongoing roles of Phox2 homeodomain transcription factors during neuronal differentiation. Development *137*, 4211–4220. https://doi.org/10.1242/dev.056747.
45. Howard, M.J., Stanke, M., Schneider, C., Wu, X., and Rohrer, H. (2000). The transcription factor dHAND is a downstream effector of BMPs in sympathetic neuron specification. Development *127*, 4073–4081.
46. Morrison, M.A., Zimmerman, M.W., Look, A.T., and Stewart, R.A. (2016). Studying the peripheral sympathetic nervous system and neuroblastoma in zebrafish. Methods Cell Biol. *134*, 97–138. https://doi.org/10.1016/bs.mcb.2015.12.003.
47. Zhang, Q., Huang, R., Ye, Y., Guo, X., Lu, J., Zhu, F., Gong, X., Zhang, Q., Yan, J., Luo, L., et al. (2018). Temporal requirements for ISL1 in sympathetic neuron proliferation, differentiation, and diversification. Cell Death Dis. *9*, 247.
48. Arendt, D., Musser, J.M., Baker, C.V.H., Bergman, A., Cepko, C., Erwin, D.H., Pavlicev, M., Schlosser, G., Widder, S., Laubichler, M.D., and Wagner, G.P. (2016). The origin and evolution of cell types. Nat. Rev. Genet. *17*, 744–757. https://doi.org/10.1038/nrg.2016.127.
49. Hnisz, D., Abraham, B.J., Lee, T.I., Lau, A., Saint-André, V., Sigova, A.A., Hoke, H.A., and Young, R.A. (2013). Super-Enhancers in the Control of Cell Identity and Disease. Cell *155*, 934–947. https://doi.org/10.1016/j.cell.2013.09.053.
50. Kanki, Y., Nakaki, R., Shimamura, T., Matsunaga, T., Yamamizu, K., Katayama, S., Suehiro, J.I., Osawa, T., Aburatani, H., Kodama, T., et al. (2017). Dynamically and epigenetically coordinated GATA/ETS/SOX transcription factor expression is indispensable for endothelial cell differentiation. Nucleic Acids Res. *45*, 4344–4358. https://doi.org/10.1093/nar/gkx159.
51. Martik, M.L., and Bronner, M.E. (2017). Regulatory Logic Underlying Diversification of the Neural Crest. Trends Genet. *33*, 715–727. https://doi.org/10.1016/j.tig.2017.07.015.
52. Saint-André, V., Federation, A.J., Lin, C.Y., Abraham, B.J., Reddy, J., Lee, T.I., Bradner, J.E., and Young, R.A. (2016). Models of human core transcriptional regulatory circuitries. Genome Res. *26*, 385–396. https://doi.org/10.1101/gr.197590.115.
53. Escurat, M., Djabali, K., Gumpel, M., Gros, F., and Portier, M.M. (1990). Differential

expression of two neuronal intermediate-filament proteins, peripherin and the low-molecular-mass neurofilament protein (NF-L), during the development of the rat. J. Neurosci. *10*, 764–784.
54. Huber, K. (2006). The sympathoadrenal cell lineage: Specification, diversification, and new perspectives. Dev. Biol. *298*, 335–343. https://doi.org/10.1016/j.ydbio.2006.07.010.
55. Huber, K. (2015). Segregation of neuronal and neuroendocrine differentiation in the sympathoadrenal lineage. Cell Tissue Res. *359*, 333–341. https://doi.org/10.1007/s00441-014-1947-0.
56. Lumb, R., and Schwarz, Q. (2015). Sympathoadrenal neural crest cells: The known, unknown and forgotten? Dev. Growth Differ. *57*, 146–157. https://doi.org/10.1111/dgd.12189.
57. Ernsberger, U., Patzke, H., Tissierseta, J.P., Reh, T., Goridis, C., and Rohrer, H. (1995). The Expression of Tyrosine-Hydroxylase and the Transcription Factors Cphox-2 and Cash-1 - Evidence for Distinct Inductive Steps in the Differentiation of Chick Sympathetic Precursor Cells. Mech. Dev. *52*, 125–136. https://doi.org/10.1016/0925-4773(95)00396-I.
58. Ernsberger, U., Reissmann, E., Mason, I., and Rohrer, H. (2000). The expression of dopamine beta-hydroxylase, tyrosine hydroxylase, and Phox2 transcription factors in sympathetic neurons: evidence for common regulation during noradrenergic induction and diverging regulation later in development. Mech. Dev. *92*, 169–177. https://doi.org/10.1016/S0925-4773(99)00336-6.
59. Espinosa-Medina, I., Jevans, B., Boismoreau, F., Chettouh, Z., Enomoto, H., Müller, T., Birchmeier, C., Burns, A.J., and Brunet, J.F. (2017). Dual origin of enteric neurons in vagal Schwann cell precursors and the sympathetic neural crest. Proc. Natl. Acad. Sci. USA *114*, 11980–11985. https://doi.org/10.1073/pnas.1710308114.
60. Espinosa-Medina, I., Outin, E., Picard, C.A., Chettouh, Z., Dymecki, S., Consalez, G.G., Coppola, E., and Brunet, J.F. (2014). Neurodevelopment. Parasympathetic ganglia derive from Schwann cell precursors. Science *345*, 87–90. https://doi.org/10.1126/science.1253286.
61. Ponzoni, M., Bachetti, T., Corrias, M.V., Brignole, C., Pastorino, F., Calarco, E., Bensa, V., Giusto, E., Ceccherini, I., and Perri, P. (2022). Recent advances in the developmental origin of neuroblastoma: an overview. J. Exp. Clin. Cancer Res. *41*, 92. https://doi.org/10.1186/s13046-022-02281-w.
62. Furlan, A., Dyachuk, V., Kastriti, M.E., Calvo-Enrique, L., Abdo, H., Hadjab, S., Chontorotzea, T., Akkuratova, N., Usoskin, D., Kamenev, D., et al. (2017). Multipotent peripheral glial cells generate neuroendocrine cells of the adrenal medulla. Science *357*. https://doi.org/10.1126/science.aal3753.
63. Kastriti, M.E., Faure, L., Von Ahsen, D., Bouderlique, T.G., Boström, J., Solovieva, T., Jackson, C., Bronner, M., Meijer, D., Hadjab, S., et al. (2022). Schwann cell precursors represent a neural crest-like state with biased multipotency. Embo J. *41*, e108780.
64. Abu-Bonsrah, K.D., Zhang, D., Bjorksten, A.R., Dottori, M., and Newgreen, D.F. (2018). Generation of Adrenal Chromaffin-like Cells from Human Pluripotent Stem Cells. Stem Cell Rep. *10*, 134–150. https://doi.org/10.1016/j.stemcr.2017.11.003.
65. Keenan, A.B., Torre, D., Lachmann, A., Leong, A.K., Wojciechowicz, M.L., Utti, V., Jagodnik, K.M., Kropiwnicki, E., Wang, Z., and Ma'ayan, A. (2019). ChEA3: transcription factor enrichment analysis by orthogonal omics integration. Nucleic Acids Res. *47*, W212–W224. https://doi.org/10.1093/nar/gkz446.
66. Lodato, M.A., Ng, C.W., Wamstad, J.A., Cheng, A.W., Thai, K.K., Fraenkel, E., Jaenisch, R., and Boyer, L.A. (2013). SOX2 Co-Occupies Distal Enhancer Elements with Distinct POU Factors in ESCs and NPCs to Specify Cell State. PLoS Genet. *9*, e1003288.
67. Hatakeyama, J., Bessho, Y., Katoh, K., Ookawara, S., Fujioka, M., Guillemot, F., and Kageyama, R. (2004). Hes genes regulate size, shape and histogenesis of the nervous system by control of the timing of neural stem cell differentiation. Development *131*, 5539–5550. https://doi.org/10.1242/dev.01436.
68. Ohtsuka, T., Sakamoto, M., Guillemot, F., and Kageyama, R. (2001). Roles of the basic helix-loop-helix genes Hes1 and Hes5 in expansion of neural stem cells of the developing brain. J. Biol. Chem. *276*, 30467–30474. https://doi.org/10.1074/jbc.M102420200.
69. Solecki, D.J., Liu, X.L., Tomoda, T., Fang, Y., and Hatten, M.E. (2001). Activated Notch2 signaling inhibits differentiation of cerebellar granule neuron precursors by maintaining proliferation. Neuron *31*, 557–568. https://doi.org/10.1016/S0896-6273(01)00395-6.
70. Akazawa, C., Sasai, Y., Nakanishi, S., and Kageyama, R. (1992). Molecular Characterization of a Rat Negative Regulator with a Basic Helix-Loop-Helix Structure Predominantly Expressed in the Developing Nervous-System. J. Biol. Chem. *267*, 21879–21885.
71. Ishibashi, M., Moriyoshi, K., Sasai, Y., Shiota, K., Nakanishi, S., and Kageyama, R. (1994). Persistent Expression of Helix-Loop-Helix Factor Hes-1 Prevents Mammalian Neural Differentiation in the Central-Nervous-System. Embo J. *13*, 1799–1805. https://doi.org/10.1002/j.1460-2075.1994.tb06448.x.
72. Zeltner, N., and Studer, L. (2015). Pluripotent stem cell-based disease modeling: current hurdles and future promise. Curr. Opin. Cell Biol. *37*, 102–110. https://doi.org/10.1016/j.ceb.2015.10.008.
73. Pomp, O., Brokhman, I., Ben-Dor, I., Reubinoff, B., and Goldstein, R.S. (2005). Generation of peripheral sensory and sympathetic neurons and neural crest cells from human embryonic stem cells. Stem Cell. *23*, 923–930. https://doi.org/10.1634/stemcells.2005-0038.
74. Chen, Y., Takita, J., Choi, Y.L., Kato, M., Ohira, M., Sanada, M., Wang, L., Soda, M., Kikuchi, A., Igarashi, T., et al. (2008). Oncogenic mutations of ALK kinase in neuroblastoma. Nature *455*, 971–974. https://doi.org/10.1038/nature07399.
75. Morris, S.W., Kirstein, M.N., Valentine, M.B., Dittmer, K.G., Shapiro, D.N., Saltman, D.L., and Look, A.T. (1994). Fusion of a kinase gene, ALK, to a nucleolar protein gene, NPM, in non-Hodgkin's lymphoma. Science *263*, 1281–1284. https://doi.org/10.1126/science.8122112.
76. Janoueix-Lerosey, I., Lopez-Delisle, L., Delattre, O., and Rohrer, H. (2018). The ALK receptor in sympathetic neuron development and neuroblastoma. Cell Tissue Res. *372*, 325–337. https://doi.org/10.1007/s00441-017-2784-8.
77. Osajima-Hakomori, Y., Miyake, I., Ohira, M., Nakagawara, A., Nakagawa, A., and Sakai, R. (2005). Biological role of anaplastic lymphoma kinase in neuroblastoma. Am. J. Pathol. *167*, 213–222. https://doi.org/10.1016/S0002-9440(10)62966-5.
78. Wellmann, A., Doseeva, V., Butscher, W., Raffeld, M., Fukushima, P., Stetler-Stevenson, M., and Gardner, K. (1997). The activated anaplastic lymphoma kinase increases cellular proliferation and oncogene up-regulation in rat 1a fibroblasts. Faseb. J. *11*, 965–972. https://doi.org/10.1096/fasebj.11.12.9337149.
79. Lambertz, I., Kumps, C., Claeys, S., Lindner, S., Beckers, A., Janssens, E., Carter, D.R., Cazes, A., Cheung, B.B., De Mariano, M., et al. (2015). Upregulation of MAPK Negative Feedback Regulators and RET in Mutant ALK Neuroblastoma: Implications for Targeted Treatment. Clin. Cancer Res. *21*, 3327–3339. https://doi.org/10.1158/1078-0432.Ccr-14-2024.
80. Claeys, S., Denecker, G., Durinck, K., Decaesteker, B., Mus, L.M., Loontiens, S., Vanhauwaert, S., Althoff, K., Wigerup, C., Bexell, D., et al. (2019). ALK positively regulates MYCN activity through repression of HBP1 expression. Oncogene *38*, 2690–2705. https://doi.org/10.1038/s41388-018-0595-3.
81. Mus, L.M., Lambertz, I., Claeys, S., Kumps, C., Van Loocke, W., Van Neste, C., Umapathy, G., Vaapil, M., Bartenhagen, C., Laureys, G., et al. (2020). The ETS transcription factor ETV5 is a target of activated ALK in neuroblastoma contributing to increased tumour aggressiveness. Sci. Rep. *10*, 218.
82. Umapathy, G., El Wakil, A., Witek, B., Chesler, L., Danielson, L., Deng, X., Gray, N.S., Johansson, M., Kvarnbrink, S., Ruuth, K., et al. (2014). The kinase ALK stimulates the kinase ERK5 to promote the expression of the oncogene MYCN in neuroblastoma. Sci. Signal. *7*, ra102. https://doi.org/10.1126/scisignal.2005470.
83. Chiarle, R., Voena, C., Ambrogio, C., Piva, R., and Inghirami, G. (2008). The anaplastic lymphoma kinase in the pathogenesis of cancer. Nat. Rev. Cancer *8*, 11–23. https://doi.org/10.1038/nrc2291.
84. Hallberg, B., and Palmer, R.H. (2016). The role of the ALK receptor in cancer biology. Ann. Oncol. *27*, iii4–iii15. https://doi.org/10.1093/annonc/mdw301.
85. Palmer, R.H., Vernersson, E., Grabbe, C., and Hallberg, B. (2009). Anaplastic lymphoma kinase: signalling in development and disease. Biochem. J. *420*, 345–361. https://doi.org/10.1042/BJ20090387.
86. Zhu, S., Lee, J.S., Guo, F., Shin, J., Perez-Atayde, A.R., Kutok, J.L., Rodig, S.J., Neuberg, D.S., Helman, D., Feng, H., et al. (2012). Activated ALK collaborates with MYCN in neuroblastoma pathogenesis. Cancer Cell *21*, 362–373. https://doi.org/10.1016/j.ccr.2012.02.010.
87. Ahmed, S., Gan, H.T., Lam, C.S., Poonepalli, A., Ramasamy, S., Tay, Y., Tham, M., and Yu, Y.H. (2009). Transcription factors and neural stem cell self-renewal, growth and

differentiation. Cell Adh. Migr. *3*, 412–424. https://doi.org/10.4161/cam.3.4.8803.

88. Keramari, M., Razavi, J., Ingman, K.A., Patsch, C., Edenhofer, F., Ward, C.M., and Kimber, S.J. (2010). Sox2 Is Essential for Formation of Trophectoderm in the Preimplantation Embryo. PLoS One *5*, e13952.
89. Rizzino, A. (2009). Sox2 and Oct-3/4: a versatile pair of master regulators that orchestrate the self-renewal and pluripotency of embryonic stem cells. Wires Syst. Biol. Med. *1*, 228–236. https://doi.org/10.1002/wsbm.12.
90. Bylund, M., Andersson, E., Novitch, B.G., and Muhr, J. (2003). Vertebrate neurogenesis is counteracted by Sox1-3 activity. Nat. Neurosci. *6*, 1162–1168. https://doi.org/10.1038/nn1131.
91. Ferri, A.L.M., Cavallaro, M., Braida, D., Di Cristofano, A., Canta, A., Vezzani, A., Ottolenghi, S., Pandolfi, P.P., Sala, M., DeBiasi, S., and Nicolis, S.K. (2004). Sox2 deficiency causes neurodegeneration and impaired neurogenesis in the adult mouse brain. Development *131*, 3805–3819. https://doi.org/10.1242/dev.01204.
92. Graham, V., Khudyakov, J., Ellis, P., and Pevny, L. (2003). SOX2 functions to maintain neural progenitor identity. Neuron *39*, 749–765. https://doi.org/10.1016/S0896-6273(03)00497-5.
93. Miyagi, S., Masui, S., Niwa, H., Saito, T., Shimazaki, T., Okano, H., Nishimoto, M., Muramatsu, M., Iwama, A., and Okuda, A. (2008). Consequence of the loss of Sox2 in the developing brain of the mouse. FEBS Lett. *582*, 2811–2815. https://doi.org/10.1016/j.febslet.2008.07.011.
94. Bertrand, N., Castro, D.S., and Guillemot, F. (2002). Proneural genes and the specification of neural cell types. Nat. Rev. Neurosci. *3*, 517–530. https://doi.org/10.1038/nrn874.
95. Kageyama, R., Ohtsuka, T., Hatakeyama, J., and Ohsawa, R. (2005). Roles of bHLH genes in neural stem cell differentiation. Exp. Cell Res. *306*, 343–348. https://doi.org/10.1016/j.yexcr.2005.03.015.
96. Yun, K., Mantani, A., Garel, S., Rubenstein, J., and Israel, M.A. (2004). Id4 regulates neural progenitor proliferation and differentiation *in vivo*. Development *131*, 5441–5448. https://doi.org/10.1242/dev.01430.
97. Alvarezbolado, G., Rosenfeld, M.G., and Swanson, L.W. (1995). Model of Forebrain Regionalization Based on Spatiotemporal Patterns of Pou-Iii Homeobox Gene-Expression, Birth-Dates, and Morphological Features. J. Comp. Neurol. *355*, 237–295. https://doi.org/10.1002/cne.903550207.
98. Hara, Y., Rovescalli, A.C., Kim, Y., and Nirenberg, M. (1992). Structure and evolution of four POU domain genes expressed in mouse brain. Proc. Natl. Acad. Sci. USA *89*, 3280–3284. https://doi.org/10.1073/pnas.89.8.3280.
99. Mathis, J.M., Simmons, D.M., He, X., Swanson, L.W., and Rosenfeld, M.G. (1992). Brain-4 - a Novel Mammalian Pou Domain Transcription Factor Exhibiting Restricted Brain-Specific Expression. Embo J. *11*, 2551–2561. https://doi.org/10.1002/j.1460-2075.1992.tb05320.x.
100. Zhu, Q., Song, L., Peng, G., Sun, N., Chen, J., Zhang, T., Sheng, N., Tang, W., Qian, C., Qiao, Y., et al. (2014). The transcription factor Pou3f1 promotes neural fate commitment via activation of neural lineage genes and inhibition of external signaling pathways. Elife *3*, e02224.
101. Hussenet, T., Dali, S., Exinger, J., Monga, B., Jost, B., Dembelé, D., Martinet, N., Thibault, C., Huelsken, J., Brambilla, E., and du Manoir, S. (2010). SOX2 Is an Oncogene Activated by Recurrent 3q26.3 Amplifications in Human Lung Squamous Cell Carcinomas. PLoS One *5*, e8960.
102. Lu, Y., Futtner, C., Rock, J.R., Xu, X., Whitworth, W., Hogan, B.L.M., and Onaitis, M.W. (2010). Evidence That SOX2 Overexpression Is Oncogenic in the Lung. PLoS One *5*, e11022.
103. Gangemi, R.M.R., Griffero, F., Marubbi, D., Perera, M., Capra, M.C., Malatesta, P., Ravetti, G.L., Zona, G.L., Daga, A., and Corte, G. (2009). SOX2 Silencing in Glioblastoma Tumor-Initiating Cells Causes Stop of Proliferation and Loss of Tumorigenicity. Stem Cell. *27*, 40–48. https://doi.org/10.1634/stemcells.2008-0493.
104. Congras, A., Hoareau-Aveilla, C., Caillet, N., Tosolini, M., Villarese, P., Cieslak, A., Rodriguez, L., Asnafi, V., Macintyre, E., Egger, G., et al. (2020). ALK-transformed mature T lymphocytes restore early thymus progenitor features. J. Clin. Invest. *130*, 6395–6408. https://doi.org/10.1172/Jci134990.
105. Gelebart, P., Hegazy, S.A., Wang, P., Bone, K.M., Anand, M., Sharon, D., Hitt, M., Pearson, J.D., Ingham, R.J., Ma, Y., and Lai, R. (2012). Aberrant expression and biological significance of Sox2, an embryonic stem cell transcriptional factor, in ALK-positive anaplastic large cell lymphoma. Blood Cancer J. *2*, e82. https://doi.org/10.1038/bcj.2012.27.
106. Cimadamore, F., Fishwick, K., Giusto, E., Gnedeva, K., Cattarossi, G., Miller, A., Pluchino, S., Brill, L.M., Bronner-Fraser, M., and Terskikh, A.V. (2011). Human ESC-Derived Neural Crest Model Reveals a Key Role for SOX2 in Sensory Neurogenesis. Cell Stem Cell *8*, 538–551. https://doi.org/10.1016/j.stem.2011.03.011.
107. Roellig, D., Tan-Cabugao, J., Esaian, S., and Bronner, M.E. (2017). Dynamic transcriptional signature and cell fate analysis reveals plasticity of individual neural plate border cells. Elife *6*, e21620.
108. Cheng, D.T., Mitchell, T.N., Zehir, A., Shah, R.H., Benayed, R., Syed, A., Chandramohan, R., Liu, Z.Y., Won, H.H., Scott, S.N., et al. (2015). Memorial Sloan Kettering-Integrated Mutation Profiling of Actionable Cancer Targets (MSK-IMPACT) A Hybridization Capture-Based Next-Generation Sequencing Clinical Assay for Solid Tumor Molecular Oncology. J. Mol. Diagn. *17*, 251–264. https://doi.org/10.1016/j.jmoldx.2014.12.006.
109. Fan, Y., Hackland, J., Baggiolini, A., Hung, L.Y., Zhao, H., Zumbo, P., Oberst, P., Minotti, A.P., Hergenreder, E., Najjar, S., et al. (2023). hPSC-derived sacral neural crest enables rescue in a severe model of Hirschsprung's disease. Cell Stem Cell *30*, 264–282.e269.
110. Love, M.I., Huber, W., and Anders, S. (2014). Moderated estimation of fold change and dispersion for RNA-seq data with DESeq2. Genome Biol. *15*, 550. https://doi.org/10.1186/s13059-014-0550-8.
111. Zheng, G.X.Y., Terry, J.M., Belgrader, P., Ryvkin, P., Bent, Z.W., Wilson, R., Ziraldo, S.B., Wheeler, T.D., McDermott, G.P., Zhu, J., et al. (2017). Massively parallel digital transcriptional profiling of single cells. Nat. Commun. *8*, 14049. https://doi.org/10.1038/ncomms14049.
112. Hao, Y., Hao, S., Andersen-Nissen, E., Mauck, W.M., 3rd, Zheng, S., Butler, A., Lee, M.J., Wilk, A.J., Darby, C., Zager, M., et al. (2021). Integrated analysis of multimodal single-cell data. Cell *184*, 3573–3587.e29. https://doi.org/10.1016/j.cell.2021.04.048.
113. Angerer, P., Haghverdi, L., Büttner, M., Theis, F.J., Marr, C., and Buettner, F. (2016). destiny: diffusion maps for large-scale single-cell data in R. Bioinformatics *32*, 1241–1243. https://doi.org/10.1093/bioinformatics/btv715.
114. Street, K., Risso, D., Fletcher, R.B., Das, D., Ngai, J., Yosef, N., Purdom, E., and Dudoit, S. (2018). Slingshot: cell lineage and pseudotime inference for single-cell transcriptomics. BMC Genom. *19*, 477. https://doi.org/10.1186/s12864-018-4772-0.
115. Aibar, S., González-Blas, C.B., Moerman, T., Huynh-Thu, V.A., Imrichova, H., Hulselmans, G., Rambow, F., Marine, J.C., Geurts, P., Aerts, J., et al. (2017). SCENIC: single-cell regulatory network inference and clustering. Nat. Methods *14*, 1083–1086. https://doi.org/10.1038/nmeth.4463.
116. Van de Sande, B., Flerin, C., Davie, K., De Waegeneer, M., Hulselmans, G., Aibar, S., Seurinck, R., Saelens, W., Cannoodt, R., Rouchon, Q., et al. (2020). A scalable SCENIC workflow for single-cell gene regulatory network analysis. Nat. Protoc. *15*, 2247–2276. https://doi.org/10.1038/s41596-020-0336-2.
117. Moerman, T., Aibar Santos, S., Bravo González-Blas, C., Simm, J., Moreau, Y., Aerts, J., and Aerts, S. (2019). GRNBoost2 and Arboreto: efficient and scalable inference of gene regulatory networks. Bioinformatics *35*, 2159–2161. https://doi.org/10.1093/bioinformatics/bty916.
118. Mootha, V.K., Lindgren, C.M., Eriksson, K.F., Subramanian, A., Sihag, S., Lehar, J., Puigserver, P., Carlsson, E., Ridderstråle, M., Laurila, E., et al. (2003). PGC-1alpha-responsive genes involved in oxidative phosphorylation are coordinately downregulated in human diabetes. Nat. Genet. *34*, 267–273. https://doi.org/10.1038/ng1180.
119. Subramanian, A., Tamayo, P., Mootha, V.K., Mukherjee, S., Ebert, B.L., Gillette, M.A., Paulovich, A., Pomeroy, S.L., Golub, T.R., Lander, E.S., and Mesirov, J.P. (2005). Gene set enrichment analysis: a knowledge-based approach for interpreting genome-wide expression profiles. Proc. Natl. Acad. Sci. USA *102*, 15545–15550. https://doi.org/10.1073/pnas.0506580102.

STAR★METHODS

KEY RESOURCES TABLE

REAGENT or RESOURCE	SOURCE	IDENTIFIER
Antibodies		
Mouse anti-human-CD49d	Biolegend	Cat#304314; RRID: AB_10643278
B0251 anti-human Hashtag 1	Biolegend	Cat#394631; RRID: AB_2814347
B0252 anti-human Hashtag 2	Biolegend	Cat#394633; RRID: AB_2814348
B0253 anti-human Hashtag 3	Biolegend	Cat#394635; RRID: AB_2814349
B0254 anti-human Hashtag 4	Biolegend	Cat#394637; RRID: AB_2814350
B0255 anti-human Hashtag 5	Biolegend	Cat#394639; RRID: AB_2814351
B0256 anti-human Hashtag 6	Biolegend	Cat#394641; RRID: AB_2814352
Rabbit anti-human Troponin T	abcam	Cat#ab228847
Mouse anti-human Brachyury	R&D systems	Cat#IC2085A; RRID: AB_2891298
Rabbit anti-human FOXG1	abcam	Cat#ab196868; RRID: AB_2892604
Mouse anti-human PAX6	BD Biosciences	Cat#562249; RRID: AB_11152956
Rabbit anti-human FOXA2	abcam	Cat#ab108422; RRID: AB_11157157
Mouse anti-human SOX17	BD Biosciences	Cat#561590; RRID: AB_10717127
Rat anti-human SOX2	Fisher Scientific	Cat#14981182; RRID:AB_11219471
Mouse anti-human PRPH (A3)	Santa Cruz	Cat#sc377093; RRID: AB_2923264
Mouse anti-human PHOX2B	Santa Cruz	Cat#sc-376997B-11
Mouse anti-human ASCL1	Santa Cruz	Cat#sc-374104D-7
Chemicals, peptides, and recombinant proteins		
Dulbecco's Phosphate-Buffered Saline	Corning	Cat#21-031-CV
DMEM/F12	Gibco	Cat#21331020
E8 medium	Gibco	Cat#A1517-001
E6 medium	Gibco	Cat#A1516-401
Neurobasal medium	Gibco	Cat#21103-049
B27 supplement	Gibco	Cat#17504-044
N2 supplement	Gibco	Cat#17502-048
MEM non-essential amino acids (NEAA)	Sigma	Cat#M7145
L-Glutamine	Gibco	Cat#25030-164
2-mercaptoethanol	Gibco	Cat#21985023
Matrigel	Fisher Scientific	Cat#08-774-552
Geltrex	Gibco	Cat#A1413-302
Poly-Ornithine	Sigma	Cat#P3655
Fibronectin	Gibco	Cat#33010-018
Mouse Laminin-1	Gibco	Cat#23017-015
Dispase	Stem Cell Technologies	Cat#07913
Accutase	Innovative Cell Technologies	Cat#AT-104
TRIzol Reagent	Thermo Fisher	Cat#15596018
Stem-Cellbanker	Nippon Zenyaku Kogyo	Cat#181218
Rock inhibitor (Y-27632)	R&D Systems	Cat#1524
SB431542	R&D Systems	Cat#1614
Chir99021	R&D Systems	Cat#4423
Fibroblast growth factor 2	R&D Systems	Cat#233-FB/CF

(*Continued on next page*)

Continued

REAGENT or RESOURCE	SOURCE	IDENTIFIER
Bone morphogenic protein 4	R&D Systems	Cat#314-BP
SHH	R&D Systems	Cat#464-SH
Ascorbic acid	Sigma	Cat#4034-100g
Nerve growth factor	Peprotech	Cat#450-01
Brain derived neurotrophic factor	R&D Systems	Cat#248-BDB
Glial cell derived neurotrophic factor	Peptrotech	Cat#450-10
Purple loading dye	NEB	Cat#B7024S
BD Cytofix fixation buffer	BD Biosciences	Cat#51-9006276
QBSF-60 medium	Fisher Scientific	Cat#NC0823508
RPMI medium	Fisher Scientific	Cat#MT10041CV
B27(-insulin)	Gibco	Cat#17504044
Fetal bovine serum (FBS)	ClonTech	Cat#631101
KO serum-replacement	Gibco	Cat#10828028
Recombinant Human Erythropoietin (EPO)	R&D Systems	Cat#287-TC-500
Recombinant Human SCF (SCF)	R&D Systems	Cat#255-SC-010/CF
Recombinant Human Interleukin-3 (IL-3)	R&D Systems	Cat#203-IL-010/CF
Insulin-like growth factor 1 (IGF-1)	R&D Systems	Cat#291-G1-200
Dexamethasone	Sigma	Cat#D88931MG
4′,6-diamidino-2-phenylindole (DAPI)	Invitrogen	Cat#D1306
IWP 2	R&D Systems	Cat#3533
Dihydrochloride (LDN)	R&D Systems	Cat#6053
Activin A	R&D Systems	Cat#338-AC
Normicine	InvivoGen	Cat#ant-nr-1
Cell staining buffer	Biolegend	Cat#420201
Human TruStain FcX™	Biolegend	Cat#422301
Critical commercial assays		
Cytotune-iPS 2.0 Sendai reprogramming kit	Life Technologies	Cat#A16517
KAPA Hyper Prep Kit	Kapa Biosystems	Cat#KK8504
AmpFLSTR Identifiler Plus PCR Amplification Kit	ThermoFisher	Cat#A26182
Mycoplasma PCR detection kit	ABM	Cat#G238
BD stemflow kit	BD Biosciences	Cat#560589
HiSeq 3000/4000 SBS Kit	Illumina	Cat#TG-410-1002
TruSeq Stranded mRNA LT Kit	Illumina	Cat#RS-122-2102
Deposited data		
Sequencing data of differentiation trajectory	This study	Database: https://data.mendeley.com/datasets/76prtz548d/draft?a=b253cfe4-eb76-4cc3-9d59-57773693ce9b
Code for sequencing analysis	This study	Database: https://github.ugent.be/DePreterLab/Sympatho-adrenergic-differentiation-track.
Experimental models: Cell lines		
Mouse embryonic fibroblasts	Gibco	Cat#A34181
Human embryonic stem cell (hESC) lines H9 (WA-09)	(Thomson, Itskovitz-Eldor et al. 1998)	RRID:CVCL_9773
H9 derived SOX10::GFP reporter line	(Chambers, Qi et al. 2012)	N/A
WA01 derived TH-tdtomato reporter line	(Ahfeldt, Tim et al. 2020)	N/A
Induced pluripotent stem cell (iPSC) line: MRC5-iPSC	Laboratory of Lorenz Studer	N/A
Human: ALK^{R1275Q} patient-specific iPSC line: NB05	This study	N/A

(*Continued on next page*)

Continued

REAGENT or RESOURCE	SOURCE	IDENTIFIER
Software and algorithms		
R-Studio Desktop (version 4.1.1)	RStudio Team (2020)	https://www.rstudio.com/
10x Genomics Cell Ranger software (version 6.0.0)	Zheng et al. 2017	https://www.10xgenomics.com/software
GRCh38 human genome (bundle 3.0.0)	Genome Reference Consortium	http://www.ncbi.nlm.nih.gov/projects/genome/assembly/grc/human/
Seurat (version 4.1.1)	Hao et al. 2021	https://satijalab.org/seurat/
destiny R package v.3.10.0	Angerer et al. 2016	https://bioconductor.org/packages/release/bioc/html/destiny.html
pySCENIC1,2	Aibar et al. 2017, Van de Sande et al. 2020	https://github.com/vib-singlecell-nf/vsn-pipelines
GRNBoost2 (SCENIC version 0.10.4)	Moerman et al. 2019	https://github.com/aertslab/GRNBoost
Gene set enrichment analysis (GSEA) v4.0.2	Subramanian et al. 2005, Mootha et al. 2003	https://www.gsea-msigdb.org/gsea/index.jsp
Biorender	Biorender	https://biorender.com/
slingshot R package v2.4.0	Street et al. 2018	https://www.bioconductor.org/packages/release/bioc/html/slingshot.html
Other		
In vivo single cell sequencing data of SAP development	Laboratory of Igor Adameyko	GSE147821

RESOURCE AVAILABILITY

Lead contact

Further information and requests for resources and reagents should be directed to and will be fulfilled by the lead contact, Stephen Roberts (roberste@ohsu.edu).

Materials availability

The patient-specific IPSC line NB05, generated in this study, is available from the lead contact upon request.

Data and code availability

- RNA-seq data have been deposited at 'Mendeley Data' and are publicly available as of the date of publication. The link to our Mendely data depository is listed in the key resources table. Microscopy data reported in this paper will be shared by the lead contact upon request.
- All original code has is provided on Github and accessible through https://github.ugent.be/PPOL/Sympatho-adrenergic-differentiation-track.
- Any additional information required to reanalyze the data reported in this paper is available from the lead contact upon request.

EXPERIMENTAL MODEL AND STUDY PARTICIPANT DETAILS

Human subjects

The patient from which NB05 was generated was enrolled on IRB-approved MSKCC institutional protocols for tumour and germline sequencing and informed consent from patients or caregivers was obtained prior to collecting blood samples.

Cell lines

- NB05: Patient-specific iPSC line generated in this study, carrying ALK^{R1275Q} mutation,[74] female. Authenticated using STR, IMPACT, sWGS and mycoplasma testing (see method details).
- H9: hESC, female
- J2 human iPSCs, male
- H9 SOX10-GFP reporter line, female
- WA01 TH-tdtomato reporter, male

Coating of culture plates

Seeding feeder-layer

MEFs (Gibco, Cat# A34181), which were mitotically inactivated with mitomycin C or γ-irradiation, were used as a feeder layer to produce the necessary growth factors for hESCs. To thaw MEFs, 1mL of cold MEF medium (Table S1) was added to a vial of frozen cells, which were then added to 10 mL medium. Cells were counted using the automatic cell counter of 'Nexcelom' and 11,000 cells/cm^2 were seeded. Following seeding, plates were gently shaken until MEFs were evenly distributed over the entire well surface. Finally, plates were incubated at 37°C and and 5% CO_2.

Coating matrigel plates

Matrigel-coated plates were prepared by thawing Matrigel (Fisher Scientific, Cat# 08-774-552) overnight at 4°C and diluting it in DMEM/F12 (1:100) (Gibco, Cat nr. 21331020). Subsequently 50-, 250-, 1000 μL of Matrigel-DMEM/F12 were added to 96-, 24-, and six-well plates respectively.

Coating geltrex

Geltrex-coated plates were prepared by thawing Geltrex (Gibco, Cat nr. A1413-302) overnight at 4°C and diluting it in DMEM/F12 (1:50). Subsequently 500-, 1000 μL of Matrigel-DMEM/F12 were added to 24-, and six-well plates respectively and the plates were left to coat at 4°C overnight.

Culturing of PSCs

Thawing of PSCs

To thaw the PSCs, we shortly placed one vial of PSCs, previously stored in liquid nitrogen, in a water bath operating at 37°C, and subsequently resuspended its cell content into 9mL E8 medium (Gibco, Cat nr. A1517001). The cells were thereafter centrifuged at 120 x g for 3 min at room temperature and resuspended in E8 supplemented with 10μM Rock inhibitor (Y-27632, R&D, Cat nr. 1524). Medium was renewed daily.

Passaging of PSCs

PSCs were maintained in E8 medium with E8 supplement in humidified atmosphere with 5% CO2 at 37°C. The cells were passaged biweekly by treatment with accutase (Innovative Cell technologies, Cat nr. AT-104) for 15min. Accutase was neutralised with E8 medium in a ratio of 3:1. The cell suspension was counted and centrifuged at 120 x g for 3 min. Eventually, 20-30,000 cells/well were seeded on previously prepared Matrigel-coated six well plates.

Freezing of PSCs

The first step of the freezing process was identical to the passaging of that for the PSCs. After centrifugation, pelleted cells from one well of a six-well plate were resuspended in STEM-CELLBANKER (Nippon Zenyaku Kogyo, Cat nr. 181218), which is a specific medium developed to optimize freezing and thawing conditions for stem cells. The cells were then placed at - 80°C in a freezing container, allowing for a decrease of 1°C/min. The following day the cells were stored in the liquid nitrogen for long-term storage.

METHOD DETAILS

Generating patient-specific iPSCs

Isolation and culture of leukocytes

Prior to sample collection, all patients were enrolled on Institutional Review Board (IRB)-approved institutional protocols accepting to sample banking, WGS, and iPS cell line generation. We reprogrammed peripheral WBCs from a familial NB patient with the *ALK*^{R1275Q} mutation. WBCs were isolated from whole blood by Ficoll density gradient centrifugation. The mononuclear cell layer was subsequently transferred to a sterile tube, washed with Dulbecco's Phosphate-Buffered Saline (DPBS, Corning, Cat nr. 21-031-CV) and stored in liquid nitrogen. Proceeding further, the WBCs were thawed into QBSF-60 medium (Fisher Scientific, Cat# NC0823508) and the numbers of viable cells were determined using the acridine orange and propidium iodide (AOPI) viability staining method on a Nexcelom K2 automated cell counter. Next, the cells were resuspended in peripheral blood mononuclear cell medium (PBMC, Table S1) and plated onto a well of ultra-low attachment six-well plates. PBMC medium was renewed every 2-3 days for 10 days.

Reprogramming of leukocytes to iPSC

For transduction of the peripheral WBCs, referred to as 'day 0', cells were counted and viable cells were transduced with Sendai virus containing OCT4, Klf4, Sox2 and c-Myc vectors from the 'Cytotune-iPS 2.0 Sendai reprogramming kit' (Life Technologies, Cat nr. A16517) according to the manufacturer's instructions. Thereafter, the cells were incubated at 37°C for 6-8 hours. After incubation, 1mL of additional PBMC medium was added into each well. On the following day (day 1), the cells were re-plated on ultra-low attachment six-well plates. On day 3, the transduced cells were resuspended in induced pluripotent stem cell (iPSC) medium (Table S1) and plated on previously prepared mouse embryonic fibroblasts (MEF)-coated six-well plates. Transition from iPSC medium to human embryonic stem cell (hESC, Table S1) medium took

place on days 5, 7 and 9. On day 5, iPSC medium was added without supplemental growth factors. On day 7, the medium was changed to a 1:1 mixture of iPSC medium and hESC medium. From day 9 onwards, the cells were cultured with hESC medium for 12-15 additional days. Between days 21-25, undifferentiated dome-like colonies with clear, smooth edges were selected and seeded onto prepared MEF-coated 24-well plates.

Transition culture on MEF to Matrigel

After generating iPSCs, they were transitioned from a culture on MEF-coated six well plates to culture on Matrigel in a one-step process. The IPSC colonies on the MEF feeder layer were treated with dispase (Stem Cell Technologies, Cat# 07913) for eight minutes. Thereafter, the dispase was replaced with 3-4 mL/well of E8 medium in a six-well plate. With the aid of a p1000 pipette, the colonies were carefully detached and slightly fragmented. 1 mL/well of iPSC suspension was transitioned to previously prepared Matrigel-coated six-well plates.

Mutation analysis

The presence of the mutation of interest and absence of co-mutations was confirmed with DNA profiling using the IMPACT (Integrated Mutation Profiling of Actionable Cancer Targets) assay.[108] This assay involves hybridization of barcoded libraries to custom oligonucleotides (Nimblegen SeqCap) designed to capture all protein-coding exons and select introns of 468 commonly implicated oncogenes, tumour suppressor genes, and members of pathways deemed actionable by targeted therapies. Barcoded sequence libraries were prepared using 59-100ng genomic DNA with the KAPA Hyper Prep Kit (Kapa Biosystems , Cat nr. KK8504) and combined in equimolar pools. The captured pools were subsequently sequenced on an Illumina HiSeq 4000 as paired-end 100-base pair reads, producing 314-fold coverage per tumour.

Shallow whole genome sequencing (sWGS)

After PicoGreen quantification and quality control by Agilent BioAnalyzer, 100-140 ng of genomic DNA were sheared using a LE220-plus Focused-ultrasonicator (Covaris catalog # 500569). Next, sequencing libraries were prepared using the KAPA Hyper Prep Kit (Kapa Biosystems , Cat nr. KK8504) with 8 cycles of PCR. Samples were run on an Illumina HiSeq 4000 sequencer (100 bp paired-end sequencing), using the HiSeq 3000/4000 SBS Kit (Illumina). The average number of read pairs per sample was 12 million.

Short tandem repeat (STR) array

After PicoGreen quantification, 500pg of genomic DNA was amplified using the AmpFLSTR Identifiler Plus PCR Amplification Kit (ThermoFisher Cat nr. A26182) according to the manufacturer's protocol in a 0.5X reaction. 1-2μL of PCR product was analyzed on the SeqStudio Genetic Analyzer (ThermoFisher) using a GeneScan 500 LIZ dye Size Standard (ThermoFisher Cat nr. 4322682). Resultant amplification peaks were analyzed using GeneMapper Software 5. Results shown in Table S2.

Mycoplasma detection

To confirm absence of mycoplasma infection in the established iPSC lines, PCR testing for mycoplasma was performed using ABM's mycoplasma PCR detection kit (ABM, Cat nr. G238). The PCR products were resolved by 1% agarose gel electrophoresis. The loading buffer was Purple loading dye (6x) (NEB, Cat nr. B7024S) and Generuler 1kb plus (Thermo Scientific, Cat nr. SM1331) was used as ladder. Following, the gels were imaged with Chemidoc XRS+ (Bio-Rad).

Validation of pluripotency of generated patient-specific iPSC

Fluorescence-activated cell sorting (FACS)

Cells were treated with Accutase solution for 30 min at 37°C in order to create a single-cell solution, which was subsequently washed with DPBS and fixed with BD Cytofix fixation buffer (BD Biosciences, Cat nr. 51-9006276) and stored at 4°C until further processing. Pluripotency of the generated iPSCs was tested by performing FACS analysis (BDFACS aria III cell sorter, Cat nr. 648282) for the expression of stem cell markers OCT3/4 and SOX2 with the BD stemflow kit (BD Biosciences, Cat nr. 560589), according to the manufacturer's protocol. In this analysis, an iPSC clone was considered pluripotent when $\geq$ 90% of the cells were positive for both of the aforementioned stem cell makers.

Tri-lineage differentiation

Meso-endoderm induction: 400,000 cells were plated onto each well in Matrigel-coated 24-well plates. Once the cells were near confluency (on average 2 days after seeding), they were treated with 10μM CHIR99021 (R&D Systems, Cat nr. 4423) in B27(-insulin)/RPMI medium (Gibco, Cat nr. 17504044, Fisher Scientific MT10041CV) for 24 hours. Two days later, the cells were treated with 5μM IWP2 (TOCRIS, Cat nr. 3533) in B27(-insulin)/RPMI medium for 48 hours (medium replacement was done every two days). Spontaneous contraction of myocardiocytes could be detected at day 9. The development of meso-endoderm was validated using immunofluorescence staining for Troponin T (abcam, Cat nr. ab228847) and Brachyury (R&D systems, Cat nr. IC2085A).

Neuroectoderm induction: At the start of the differentiation, 400,000 cells were seeded onto each well in Matrigel-coated 24-well plates. The cells were plated in in E6 medium (Gibco, Cat nr. A1516401), containing 500nM LDN (TOCRIS, Cat nr. 6053) and 10μM SB (R&D Systems,

Cat nr. 1614). Medium was renewed daily for seven days. The development of neuroectoderm was validated using immunofluorescence staining for FOXG1 (abcam, Cat nr. ab196868) and PAX6 (BD Biosciences, Cat nr. 562249).

Definitive endoderm induction: At the start of the differentiation, 100,000 cells were plated onto each well in Matrigel-coated 24-well plates. Once the cells were nearly confluent, they were treated with 100 ng/mL Activin A (R&D systems, Cat nr. 338-AC) and 3μM CHIR99021 diluted in RPMI medium. The next day the medium was changed to 100 ng/mL Activin A in 0,2%fetal bovine serum/RPMI medium, which was renewed daily for three days. The development of endoderm was validated using immunofluorescence staining for FOXA2 (abcam, Cat nr. ab108422) and SOX17 (BD Biosciences, Cat nr. 561590).

Differentiation of PSC to hSAPs

Generation of truncal neural crest

In accordance to the protocol developed by the Studer lab[109] PSC were transitioned to truncal neural crest cells (truncal NCC) in a 16-day long process. First cells were seeded on geltrex coated 24 well plates at a concentration of 100k/cm^2 in medium consisting of E6 supplemented with 10μM Rock inhibitor. After allowing the cells to attach for 24hrs the medium was changed to induction medium 1 (see Table S3) for the following 2 days. Hereafter the medium was adjusted to induction medium 2 (see Table S3) which was used until D16 where we enriched for NCC using FACS sorting.

Enriching neural crest cells by FACS sorting

To enrich for NCC we selected cells with high SOX10 expression. To accomplish this the surface marker CD49d (positively correlating with SOX10 expression) was stained using CD49d-PE-Cy7 antibodies (Biolegend, Cat nr. 304314). We first detached the cells by incubating them with Accutase for 25 mintues at 37°C. Afterwards the Accutase was diluted using a 2/3 ratio of DMEM/F12 and the cells were centrifuged for 5minutes at 120g. Subsequently the cells were washed with DMEM/F12 and centrifuged at 120g for 5 minutes, this step was repeated once more for a second wash. Next the cells were stained with 35μl of CD49d-PE-Cy7 antibodies with an incubation time of 25 minutes at 4°C. Thereafter the cells were washed 3 more times with DMEM/F12. After the final wash the cells were resupended in E6-medium, containing 1:1000 Normicine (InviviGen, Cat nr. Ant-nr-1) and (1:1000) rock inhibitor, at a cell concentration of 10 million/ml. To this cell solution DAPI was added ad viability control. Subsequently the cells were FACS sorted (BDFACS aria III cell sorter, Cat#648282), based on PE-Cy7 signal. After sorting the cells were centrifuged and resuspended in spheroid medium (see Table S3). The cells were subsequently plated out on ultra-low attachment plates (Corning, Cat Nr. 3471) to generate spheres and allow for larger increase of cell numbers. The spheres were allowed to grow for 4 days after which they were plated on previously prepared PO/FN/LM coated 24 well plates.

Coating post-FACS differentiation plates

During the sphere stage Poly-Ornithine (PO, Sigma Cat Nr. P3655) was thawed overnight at 4°C, diluted to 15μg/mL in PBS and allowed to coat overnight at 37°C. Simultaneously Fibronectin (FN, Gibco, Cat nr. 33010-018) and Mouse Laminin-1 (LM, Gibco, Cat nr. 23017-015) were thawed at 4°C overnight. The next day the PO coated plates were washed and FN and LM, diluted to 2μg/mL in PBS, were added and allowed to coat overnight at 37°C.

Inducing SAP development and maturation

24Hrs after plating out the spheres the medium was changed to priming medium for a total of 4 days (see Table S3), renewed every 2 days. This priming medium mimics the stage where the truncal NCC reach the ventral side of the dorsal aorta and are exposed to BMP4 signalling. This induces a cascade of signalling consisting of transcription factors (TFs) and core regulatory circuits (CRC), such as the expression of pro-neural genes such as ASCL1 (MASH1/HASH1), and lineage-determining TFs (i.e., Phox2B, Hand2, TBX2, and SOX11) which control cell fate decisions and development of the SAP's. Subsequently the medium is changed to SNS differentiation medium (see Table S3). This was re-newed every 4 days until the end of the differentiation.

Immunofluorescence (IF) imaging

At the desired timepoints during the differentiation cells were fixed with 4% PFA for 20 at room temperature. Subsequently the cells were washed with twice PBST (consisting of PBS with 0.1% triton X100) and thereafter incubated with PBST/GS (PBST with 5% goat serum) for one hour at room temperature. Next the primary antibody was added at 4°C overnight. The primary antibody was diluted in PBST/GS at a dilution of 1:200 for *SOX2* (eBioscience, Cat nr. 14-9811-82) *PHOX2B* (Santa Cruz, Cat nr. sc-376997B-11) and *PRPH* (Santa Cruz, Cat nr. sc-377093) and 1:1000 for *ASCL1* (Santa Cruz, Cat nr. sc-374104D-7). After overnight incubation the cells were washed trice with PBST after which the secondary antibody was added for a duration of 2hrs at room temperature in the dark. Once the secondary antibody incubation was completed the cells were washed twice with PBST after which DAPI (diluted 1:10.000 in PBS) was added for 5 minutes. Subsequently the cells were washed two more times with PBS and imaged using.

Bulk RNAseq

Cell pellets were snapfrozen for analysis at selected time-points over the differentiation process. To extract RNA from the cells, phase separation in cells lysed in TRIzol Reagent (ThermoFisher Cat Nr. 15596018) was induced with chloroform. RNA was precipitated with isopropanol

and linear acrylamide and washed with 75% ethanol. The samples were resuspended in RNase-free water. After RiboGreen quantification and quality control by Agilent BioAnalyzer, 125-500ng of total RNA with an RNA integrity number varying from 7.8-10 underwent polyA selection and TruSeq library preparation according to instructions provided by Illumina (TruSeq Stranded mRNA LT Kit, Cat Nr. RS-122-2102), with 8 cycles of PCR. Samples were barcoded and run on a HiSeq 4000 in a 50bp/50bp paired end run, using the HiSeq 3000/4000 SBS Kit (Illumina Cat nr. TG-410-1002). An average of 39 million paired reads was generated per sample. At the most, the ribosomal reads represented 1.9% of the total reads generated and the percent of mRNA bases averaged 67%. The counts per gene were normalized using DESeq2.[110] The counts for each gene in each sample is divided by the geometric mean of the gene across all samples. The median of the ratios for the genes in a sample is the estimated size "scaling" size factor used to adjust the total mapped reads count from each sample.

Cell hashing

Prior to scRNAseq the cells of selected time-points were hashed and pooled together for scRNAseq analysis. The time-points D25-26, D27-28, D29-30 and D31-32 were hashed for the WT cells. For the ALK mutant cells time-points D25-27-29-32 were hashed. After dissociating the cells with Accutase for 25 minutes we prepared a 50µl single cell suspension at a concentration between 1x105 cells/mL and 2x107 cells/mL for each hasing group in Cell Staining Buffer (BioLegend, Cat nr. 420201) for cell labelling. 5µl Of cell solution was used to record total cell count and cell viability using Trypan Blue. To the remaining 45µl, 0.1X volume (5 µL) of Human TruStain FcX (BioLegend, Cat nr. 422301) was added. This was allowed to incubate for 10 minutes at 4°C. During this incubation time a solution of 1µg /50µl was prepared for each hashing antibody (B0251 – B0256, see key resources table). The hashing antibody solution was centrifuged at 14,000g at 4°C for 10 minutes. The antibody solution was thereafter carefully withdrawn, whilst avoiding touching the bottom of the tube, and transferred on the corresponding cell solution. This was allowed to incubate for 30 minutes at 4°C, simultaneously the cell staining buffer was cooled down to 4°C. After incubation the cell solution was diluted 10 times by adding 0.9 mL cell staining buffer and transferred to a 12 x 75mm Falcon Round-Bottom Polystyrene Tube. Subsequently we added 2.5ml of cell staining buffer for a final dilution of 35 times. The cell solutions where thereafter centrifuged at 400g at 4°C for 5 minutes. Next the supernatant was aspirated leaving 50-100µl, this was repeated two more times for a total of 3 washes. It is very important to perform these washes carefully, leaving as little supernatant as possible. After the last wash the different cell solutions (each with their own hashtag) were combined into one tube, centrifuged and resupsended in DMEM-F12, as this medium was compatible with the 10XGenomics pipeline, for a final concentration of 1000 cells/µl.

10X genomics data generation and sequencing

The single-cell RNA-Seq was performed on Chromium instrument (10X genomics) following the user guide manual (Reagent Kit 3' v3.1). Each sample, containing approximately 10,000 cells at a final dilution of ~1,000 cells/µl was loaded onto the cartridge following the manual. The viability of cells was above 80%, as confirmed with 0.2% (w/v) Trypan Blue staining (Countess II). The individual transcriptomes of encapsulated cells were barcoded during RT step and resulting cDNA purified with DynaBeads followed by amplification per manual guidelines. Next, PCR-amplified product was fragmented, A-tailed, purified with 1.2X SPRI beads, ligated to the sequencing adapters and indexed by PCR. The indexed DNA libraries were double-size purified (0.6–0.8X) with SPRI beads and sequenced on Illumina NovaSeq S4 platform (R1 – 26 cycles, i7 – 8 cycles, R2 – 70 cycles or higher).

Biological replicates in experimental design

In the first stage of the differentiation (day 0 – day 16), immunofluorescence analysis of the H9:SOX10-GFP reporter cell line confirmed the expression of SOX10, starting from day 12 and increasing towards day 16, in three independent experiments. On day 16, FACS enrichment for SOX10+ cells on four separate PSC lines (H9 hESCs, H1 hESCs, J2 iPSCs and NB05 iPSCs), resulting in a total of 23 independent experiments, showed a stable efficiency at an average of 30%. During the second stage of the differentiation (day 21 – day 40), the H1:TH-TdTomato reporter cell line was used to analyze the expression of TH in two independent experiments. This immunofluorescence analysis confirmed TH expression starting from day 28, which continued to increase as the differentiation progressed. More in depth validation of the model was done using bulk RNA sequencing on two separate cell lines (H9 hESCs and J2 iPSCs) with two independent experiments for each cell line, resulting in a total of four independent experiments for 13 time-points covering the entire differentiation trajectory. This allowed us to identify a developmental window beginning on day 25 (after SAP induction) and ending on day 32. Within this time window, we performed single cell sequencing for J2 iPSCs at eight time-points and NB05 iPSCs at four time-points. For each time-point, separate independent experiments were conducted, and every time-point consisted of two separate differentiations pooled together. Every time-point showed a clear and consistent overlap of the populations for both cell lines, with the notable exception of the unique population identified in NB05. The identified populations were confirmed using two independent published datasets containing *in vivo* human SAP developmental data. This overlap of the SAP developmental populations allows every time-point to serve as an independent replicate, thereby confirming the robustness of the model in scRNA seq experiments with 12 independent experiments over 2 separate cell lines (J2 iPSCs and NB05 iPSCs). An overview of the replicates can be found in Table S4.

QUANTIFICATION AND STATISTICAL ANALYSIS

Gene and HTO quantification

The sequenced libraries from 14 samples were quantified with Cell Ranger software (version 6.0.0)[111] with default parameters. The standard reference provided with Cell Ranger (version 2020-A) was used. This version was built on a GRCh38 human genome (bundle 3.0.0) and a filtered version of Gencode v32. In addition, HTO surface antibodies were quantified with the Cell Ranger count feature reference option. The feature reference file is provided on GitHub.

Quality control, normalization and integration

The count files were loaded in R and further analysis with Seurat (version 4.1.1)[112] was performed. Cells with less than 300 or more than 4000 detected genes or with more than 10% mitochondrial genes were omitted. The combined dataset contained 49217 cells. Subsequently, demultiplexing of the mixes was executed by HTODemux function and only singlet were retained. The data was normalized and scaled with the standard Seurat functions. The public data (GSE147821) of Adameyko (2021) describes the complexity and tumor potential of human embryonic sympatho-adrenal area including neural crest and mesodermal derivatives in neuroblastoma tumors. Those cells was filtered with the same cut-offs and an identical normalization strategy was applied. Subsequently, the public data and own samples were integrated by making use of the Seurat integration features. On the complete data, a PCA was estimated on the top 2000 variable genes. Clustering was performed on 20 principal component dimensions (selected by visual analysis of an Elbowplot) and a resolution of 0.6. An uniform manifold approximation and projection (UMAP) embedding was calculated using the selected 20 principal components as input. Cell cycle was not regressed out. Clusters subjected to further in-depth analysis (SCP, Bridging, CPC, SAP and proliferating SAP) were extracted, re-embedded and reclustered, followed by a second post-clustering quality control phase.

Cell type annotation

Marker genes that defined clusters by differential expression were identified using the Seurat FindAllMarkers function. Clusters were annotated to cell types by comparison of marker genes for each cluster to canonical cell type markers from the literature.

Pseudotime analysis

The destiny R package v.3.10.0[113] was used to calculate the diffusion map embeddings. Single-cell pseudotime trajectories were constructed using the slingshot R package v2.4.0[114] based on clusters identified by Seurat and the DC components from destiny. A node in cluster 12 (SCPs) was selected as the starting point for the trajectory.

Regulatory program activity in single cells

Regulatory programs and their activity were inferred using pySCENIC1,2,[115,116] which was run through a Nextflow pipeline available at https://github.com/vib-singlecell-nf/vsn-pipelines with default parameters. The coexpression modules were run by GRNBoost2 (SCENIC version 0.10.4).[117] The input was the normalized expression matrix of the integrated cells across all time points after selecting and re-clustering the transcriptomes of the identified SCP, bridging, CPC and sympathoblast cells in a similar fashion as the original dataset. For plotting the regulon activity scores (RAS) in the heatmap, we retained regulons active in at least 1% of the cells and with a Pearson correlation coefficient with any other regulon greater than 0.5. RAS were normalized and rescaled in a range from 0 to 1. In parallel, we computed the Regulon Specificity Scores (RSS) for every cell type to quantify the specificity of the regulons3. For every cell type, the 20 highest scoring regulons were retained and used as input for building the network figure with CytoScape4.

Gene set enrichment analysis

The bulk RNA expression profiles of day 16 and day 35 were analysed by GSEA.[118,119] GSEA was performed using the GSEA v4.0.2 software. The genesets 'Descartes_fetal_adrenal_chromaffin_cells', 'Descartes_fetal_adrenal_sympathoblasts', 'Descartes_main_fetal_sympathoblasts' and 'GOPB_Peripheral_Nervous_system_Neuron_Differentiation' were used for enrichment of the SAP developmental cells. For enrichment of the Osteoblasts, Melanocytes and chondrocytes we used the datasets 'GOBP_Osteoblast_Development', 'GOBP_Melanocyte_Differentiation', 'GOBP_Chondrocyte_Development', respectively. All used genesets were obtained from the GSEA website (www.broadinstitute.org/gsea/). We visualised the GSEA results using enrichment map. Enrichment score (ES) and False discovery rate (FDR) value were applied to sort and select enriched genesets after gene set permutations were performed 1000 times for the analysis.